國立臺灣大學電機資訊學院電子工程學研究所

碩士論文

Graduate Institute of Electronics Engineering

College of Electrical Engineering and Computer Science

National Taiwan University

Master Thesis

氧化鋁鈍化層對金屬絕緣層半導體穿隧二極體的影響與其在感光應用之研究

Effect of Al$_2$O$_3$ Passivation (AOP) on the Characteristics of Metal-Insulator-Semiconductor (MIS) Tunnel Diodes and Its Application on Light Sensing

林彥瑜

Yen-Yu Lin

指導教授：胡振國 博士

Advisor: Jenn-Gwo Hwu, Ph.D.

中華民國 112 年 1 月

January, 2023

國立臺灣大學碩士學位論文
口試委員會審定書
MASTER'S THESIS ACCEPTANCE CERTIFICATE
NATIONAL TAIWAN UNIVERSITY

氧化鋁鈍化層對金屬絕緣層半導體穿隧二極體的影響與其在
感光應用之研究

Effect of Al$_2$O$_3$ Passivation (AOP) on the Characteristics of Metal-
Insulator-Semiconductor (MIS) Tunnel Diodes and Its Application on
Light Sensing

本論文係林彥瑜（R09943063）在國立臺灣大學電子工程學研究所完
成之碩士學位論文，於民國112年01月06日承下列考試委員審查通過
及口試及格，特此證明。

The undersigned, appointed by the Graduate Institute of Electronics Engineering on 06 January 2023
have examined a Master's thesis entitled above presented by Yen-Yu Lin (R09943063) candidate and
hereby certify that it is worthy of acceptance.

口試委員 Oral examination committee：

（指導教授 Advisor）

系主任/所長 Director：

誌謝

回顧就讀研究所的這段時間，一路上受到許多人的協助與支持，在論文正文開始之前，我想先對於這些師長、同學和朋友們表達由衷的感謝。

首先我想感謝我的指導教授—胡振國博士，無論是通過老師開設的課程或是每次 meeting 的討論，都使得我在專業知識上有很大的成長，並且老師對於研究的熱忱與專業的分析能力讓我相當敬佩，為了隨時與我們討論與修正研究的方向與提供分析數據的建議，總是不厭其煩地每周與我們進行個人 meeting，對於研究上提供了非常大的幫助，並且在給予指導的同時也給予學生足夠的空間去探索一切，真的非常感謝教授這段時間的照顧。我也想特別感謝吳幼麟教授以及胡璧合教授，在百忙之中願意擔任口試委員並給予論文修改建議，使論文得以更加完善。

感謝實驗室的學長姐、同學、學弟妹的協助。謝謝陳柏均、楊詠竣、林冠文、陳冠竹、林建宇、陳人豪學長們以及黃琛云學姊的教導與幫助，使我能夠順利度過新人時期，使我學習到許多實驗上的細節，並且與你們的討論對於研究有很大的幫助。林津丞、林俊諭、黃崧瑋同學，與你們一起修課、在無塵室做實驗的時光會是我永生難忘的回憶，中間遇到儀器出狀況研究停擺或是實驗上遇到瓶頸時，還好有大家能夠相互扶持，也謝謝你們總是不吝於給予建議與關心，尤其是黃崧瑋同學對於本論文的模擬部分提供了相當大的協助，真的由衷地感謝；也謝謝高綺憶、林郁芹學妹與陳舜啟、林軒毅、沈祐德學弟，一起修課與做實驗的經驗也是我珍貴的回憶，感謝在有需要時總是給予協助，也希望你們在研究與未來的規劃上都可以事事如意。也感謝其他的學弟妹，在最後的準備口試期間內給予的修改建議，也祝各位可以研究順利。

感謝我的家人，一路上你們的支持對我來說很重要，無論是在實質上還是精神上都給予許多支持，給我很大的自由去摸索並追尋自身的目標，遇到困難時只要想到你們心裡就得到很大的安慰，並有力量在去面對一切，沒有你們就沒有現在的我。同時，我還想特別感謝我的摯友蘇禾雅、林軒仔和陳渝方，謝謝你們總是願意聆聽煩惱並安慰我，我們的嘮叨飯局是最解壓的時間，雖然我們都在不同的領域中奮鬥，但有你們的支持我才能持續的向前進，你們就像是我家人一樣，希望我們未來都能達到各自的目標，往更美好的生活前進，蘇禾雅、陳渝方祝我們畢業快樂，林軒仔希望你一切順利，明年就換我對你說畢業快樂啦。

時光飛逝，不知不覺中兩年多的碩士時光要走到結尾，在書桌前為期末考埋頭熬夜苦讀、在如精神時光屋的無塵室裡跑製程……等等，那些當下覺得有些頭疼的時光回想起來卻變得十足珍貴，若沒有當時的努力就無法有這麼多的成長，並且在這段時間裡學會如何照顧好自己的身體與心理，所以在最後我也想好好謝謝自己，感謝過去與現在的自己，未來會繼續朝自己理想的人生前進吧。

林彥瑜
2023.01

摘要

本篇論文探討了氧化鋁鈍化層對於金屬絕緣層半導體(MIS)穿隧二極體的電性表現的影響，此元件的結構為在 MIS 穿隧二極體外圍成長上氧化鋁層作為鈍化層，我們發現到這樣的元件有著對於周圍少數載子變化十分敏感的特性，因此將其應用於感光上。在第二章中，我們對於其電容對電壓與電流對電壓兩種電性行為進行量測，發現到氧化鋁鈍化層會使得一般 MIS 穿隧二極體的深空乏行為被抑制，並且在相同氧化層厚度的情況下其在反轉區可以得到較大的電流，我們認為這樣的行為源自於鈍化層會強化元件周邊電場，使得在氧化層的壓降提升，穿隧電流因此增加。第三章中我們則對於此元件在感光上的表現進行探討，發現此元件因為外圍電場的增強可以對於周邊載子的變化變得更為敏感，無論是在電容、電流在不同光強度下相較於單純的對照組穿隧二極體有更明顯的反應，因此我們透過氧化鋁鈍化層可以進一步提升 MIS 穿隧二極體元件對於光偵測的敏感度，使其成為一個更好的感光元件選擇。

關鍵詞：金氧半穿隧元件、高介電常數、陽極氧化技術、光感測器

I

ABSTRACT
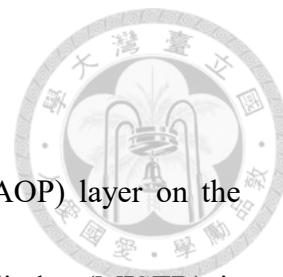
In the thesis, the influence of aluminum oxide passivation (AOP) layer on the electrical characteristics of metal-insulator-semiconductor tunnel diodes (MISTD) is investigated. The structure of this device contains an AOP layer surrounding MISTD. It is observed that AOP-MIS device is sensitive to the minority carrier change, and therefore we propose to use it as a light sensor. In Chapter 2, the capacitance versus gate voltage and current versus gate voltage are measured. It was found that the deep depletion behavior happening in MISTD device would be suppressed. Furthermore, larger current in inversion region is also observed in AOP-MIS device. We consider the reason of this behavior is originated from the enhancement of fringing field caused by AOP layer. Therefore, the voltage drop on the oxide layer becomes larger and leads to increase of tunneling current. In Chapter 3, light sensing performance of this device is studied and discussed. It is found that due to the larger fringing field, the sensitivity of the variation of extra carriers is increased. The differences of both capacitance and current show more obvious change than MISTD under light and dark condition. Consequently, it is considered that we can further increase the light sensitivity of MISTD with the help of AOP layer, and make it a better choice of light sensing.

Keyword: MIS tunneling diodes, high-k material, anodization method, light sensor

CONTENTS

Figure Captions

Chapter 1
Introduction

1-1 Motivation and Thesis Organization

The semiconductor industry has greatly changed human's life, and sped up the development of technology. According to Moore's law [1], which is proposed in 1964, the number of transistors in integrated circuit would double every 18 months. However, in recent days, whether the development of semiconductor industry still follow the Moore's law or not becomes controversial because as the device sizes are shrunk, there are some problem starting to show up such as short channel effect (SCE), narrow channel effect (NCE), drain induced barrier lowering (DIBL), etc. Therefore, there are more and more devices with new structure were proposed aiming to keep up Moore's law such as fin field-effect transistor (FinFET), gate-all-around field-effect transistor (GAAFET), and devices with different high-k material as gate dielectric. Also, metal-insulator-semiconductor (MIS) devices with ultra-thin oxide were also proposed and investigated. It is found that their current behavior are similar to Schottky diode [2], and have high sensitivity to minority carrier, which originate from the tunneling effect. With such electrical characteristics, it can be used as temperature sensor [3] - [4], memory [5] - [7], and light sensor [8].

In this thesis, some basic mechanism and fabrication method of MISTD is reviewed, and a new structure of MISTD with aluminum oxide passivation layer is proposed and investigated. In the first chapter, we will introduce the fabrication method of anodization

process and the determination method of ultra-thin oxide thickness, discuss the dependency of current on oxide thickness, and how additional minority charges supply influences the device. Also, the light sensor applications discussed in previous research is also introduced. As for the second chapter, the capacitance and current behavior of the newly proposed Al_2O_3 passivated metal-insulator-semiconductor (AOP-MIS) devices is displayed and discussed. It is observed that AOP-MIS devices can reach higher saturation current with the help of aluminum oxide layer. In chapter 3, the measurement of the light responsibility of AOP-MIS devices is presented. It was found that because aluminum oxide layer enhanced the local electric field, the sensitivity of minority carrier increases. Therefore, the devices have great sensitivity of light compared to conventional MIS devices.

1-2 Anodization system

It is found that comparing to conventional thermal oxidation process, the oxide layer fabricated by anodization process has higher quality, and the oxide thickness can be well controlled. The process was first proposed by P. F. Schmidt and W. Michel in 1957 [9]. By using anodization system, the leakage current of MOS devices with ultra-thin oxide grown through anodization system is greatly lowered and therefore the devices could have better performance [10].

The schematic diagram of anodization system is depicted in Fig. 1-1. The platinum
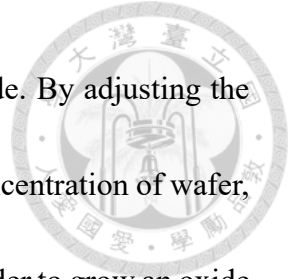
plate is connected to cathode while silicon wafer is on the anode side. By adjusting the

applied D.C. voltage, temperature, oxidation duration and doping concentration of wafer,

the growth rate and quality can be well controlled. Furthermore, in order to grow an oxide

layer with different thickness on the same wafer, wafer could be tilted so that the distance

between anode and cathode is different from place to place, leading to different electric

field over the wafer. The process can be expressed as follows:

1. In the cathode, D.I water would dissociates into hydrogen ions and hydroxide.

$$H_2O \rightleftarrows H^+ + OH^- \qquad (1\text{-}1)$$

2. Within silicon wafer, holes would be supplied from the bulk to the Si surface.

$$Si + 2h^+ \rightarrow Si^{2+} \qquad (1\text{-}2)$$

3. Then, the silicon reacts with the hydroxide and becomes silicon hydroxide.

$$Si^{2+} + 2OH^- \rightarrow Si(OH)_2 \qquad (1\text{-}3)$$
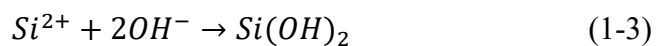
4. Finally, the silicon hydroxide would release hydrogen and form silicon dioxide.

$$Si(OH)_2 \rightarrow SiO_2 + H_2 \qquad (1\text{-}4)$$
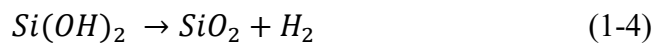
The overall reaction can be described as:

$$Si + 2h^+ + 2H_2O \rightarrow SiO_2 + H_2 + 2H^+ \qquad (1\text{-}5)$$
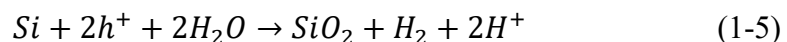
The devices in this work was under the same condition that applied D.C voltage =

15 V for 7.5 minutes in room temperature. It is also noted that to improve oxide quality,

the wafer should go through rapid thermal process (RTP) to decrease the number of

defects in the oxide layer.

1-3 Oxide Thickness Determination

For the conventional MIS devices which oxide thickness is typically larger than 3nm,

the oxide thickness can be determined by capacitance in accumulation region, which can

be expressed as [11]:

$$C_{total}(acc) \cong C_{ox} = A\frac{\varepsilon_{ox}}{d_{ox}} \qquad (1\text{-}6)$$

where A stands for the area of MIS device, ε_{ox} is the permittivity of silicon dioxide, and

d_{ox} is the thickness of oxide layer. However, for the oxide layer thinner than 3nm, the

importance of direct tunneling effect increases and the quasi-static capacitance becomes

hard to measure. Therefore, two-frequency correction method is proposed by K. Yang [12]

to make better determination of oxide thickness. The circuit model of MIS capacitor and

its equivalent parallel mode is shown in Fig. 1-2. The total impedance can be written as:

$$Z = R_s + \frac{R_p(1-j\omega CR_p)}{1+\omega^2 C^2 R_p{}^2} \qquad , \qquad (1\text{-}7)$$

where R_p is the shunt resistance, R_s is the series resistance of the substrate and the gate,

and C is the corrected capacitance. As for the parallel mode of MIS devices, the total

impedance can be expressed as an equation of measured capacitance C', and measured

resistance R'. The equation is

$$Z = \frac{D'-j}{\omega C'(1+D'^2)}, \qquad (1\text{-}8)$$

where D'= 1/ωR'C' is the dissipation factor. By equating imaginary part of two equations,

5

the relations can be obtained.

$$\frac{1+\omega^2 C^2 R_p{}^2}{C^2 R_p{}^2} = \omega C'(1 + D'^2)$$ (1-9)

Consequently, with the measured capacitance and dissipation factor of two different frequency, we can solve the actual capacitance C by subtracting two equations which can be written as:

$$C = \frac{f_1{}^2 C'_1\left(1+D'_1{}^2\right) - f_2{}^2 C'_2\left(1+D'_2{}^2\right)}{f_1{}^2 - f_2{}^2}$$ (1-10)

where C'_1 and D'_1 is the capacitance and dissipation factor measured under frequency f_1, while C'_2 and D'_2 is the capacitance and dissipation factor measured under frequency f_2.

Also, a capacitance-voltage (C-V) simulator in which a quantum mechanical effect had been taken into consideration was proposed by K.Yang, Y. C. King, and C. Hu [6], [13]. We can also extract the oxide thickness by fitting the experimental results to the simulated C-V curves.

1-4 Characteristics of p-type MIS Tunnel Diodes

1-4-1 SBH Modulation and Oxide Thickness Dependency

In previous studies, it was found that p-type MIS devices with ultra-thin oxide layer, thinner than 35Å exhibits different electrical characteristics from normal MIS device. Due to the thin oxide thickness, the voltage drop on the oxide becomes small, and the direct tunneling effect rather than Fowler-Nordheim (FN) tunneling dominates [14] - [15]. The

6

current density-voltage (J-V) curves are shown in Fig. 1-3 [16]. When the gate bias is negative, the device is under accumulation region, the current would decrease as the oxide thickness becomes larger due to the lower tunneling rate of carriers. While under positive gate bias, the saturation current is larger for devices with thicker oxide layer, which shows opposite trend to the accumulation current. To explain the saturation behavior, the Schottky barrier height (SBH) modulation was introduced [2]. In this region, the current is mainly dominated by Schottky diode hole current, which can be expressed as [17] - [18] :

$$I_h = A^* A_{eff} P_t T^2 \exp(-q\varphi_h^*/kT) \qquad (1\text{-}11)$$

where A^* represent the effective Richardson constant, A_{eff} is effective area, P_t is the tunneling probability, and φ_h^* is the effective Schottky barrier height of holes. The Schottky barrier height is related to voltage on oxide layer, which can be written as:

$$\varphi_h^* = \chi_{Si} - \Phi_m + \frac{E_g}{q} - V_{ox} \qquad (1\text{-}12)$$

where $q\chi_{Si}$ is electron affinity of silicon, $q\Phi_m$ is work function of metal (aluminum in this work), E_g is the bandgap of silicon, and V_{ox} is the oxide voltage.

The schematics diagrams of devices with thin oxide and thick oxide are depicted in Fig. 1-4. For thinner oxide, the voltage drop on the oxide layer is smaller, so the Schottky barrier height is higher, which leads to lower tunneling rate of carriers and lower saturation current. On the contrary, the device with thicker oxide can have lower Schottky

7

barrier height under the same applied gate voltage, and hence have higher saturation current.

1-4-2 Additional Minority Charges Supply

The research of effect of additional minority charges supply was also conducted previously [19]. It is found that with the lateral minority carriers generated by light, the effective Schottky barrier height would be lowered. The effective Schottky barrier height can be expressed as:

$$\varphi_h{}^* = \varphi_{h0} - \Delta\varphi_h \qquad (1\text{-}13)$$
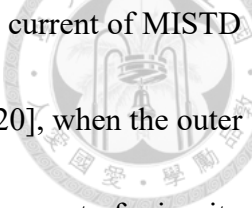
where φ_{h0} represents the original Schottky barrier height without lateral minority charges supply, while $\Delta\varphi_h$ is the change of Schottky barrier height. Also, $\Delta\varphi_h$ is related to minority carriers flux, and can be written as:

$$\Delta\varphi_h = Bq|F|d_{ox} \qquad (1\text{-}14)$$

in which B is a constant, F is lateral minority carriers flux, and d_{ox} is the thickness of oxide layer. The band diagrams of MIS devices in dark and light condition are depicted in Fig. 1-5. With light-generated minority carriers, $\varphi_h{}^*$ decreased and hence there is more holes able to tunneling through the oxide layer, which leads to larger current.

1-5 Light Sensing Application of MIS Devices

Due to the Schottky barrier height modulation affected by minority carriers supply as discussed in the last section, the MISTD has good sensitivity in light [19]. In previous

8

studies [2], it is also found that with an additional outer gate, the dark current of MISTD may be controlled by the applied gate voltage. As shown in Fig. 1-6 [20], when the outer gate voltage is set at around the flat band voltage ($V_{FB} \approx -0.9V$), the amount of minority carriers flowing toward the center MIS, which is the main sensing region, is suppressed. Consequently, the effective Schottky barrier height becomes higher, and the dark current decreases, which therefore gives rise to the increment of the I_{light}/I_{dark} ratio. Afterwards, exchange of gate and sensor regions to enhance the sensitivity was proposed by C. Y. Huang [21]. It is showed that the coupling mechanisms are asymmetric for the inner gate outer sensor (IGOS) and the inner source outer gate (ISOG) devices, which leads to different results of responsivity in light as shown in Fig. 1-7 [21]. It can be observed that under the IGOS operation condition, the device is less controlled by the gate coupling effect, and the photovoltaic effect becomes more obvious. Also, IGOS device mainly senses light with its outer ring, which has larger radius comparing to ISOG and single MIS device, and hence it can be the most sensitive among three kinds of devices.

Although researches concerning to light sensing of pure MISTD has been conducted, how high-k passivation layer may affect light sensing ability of MIS devices has not been fully studied yet. Therefore, in this thesis, a new structure of AOP-MIS device was proposed. We would discuss the differences of electrical characteristics from MIS devices, and examine its light sensing performance in the next two chapters.

9

1-6 Summary

In this chapter, the motivation and the organization of this thesis are introduced. The method of anodization process to grow high quality silicon dioxide and the determination of oxide layer thickness are explained as well. The electrical characteristics of MISTD such as SBH model and minority carrier supply are also discussed. Finally, some previous studies about MISTD used as light sensor is also introduced in the last section.
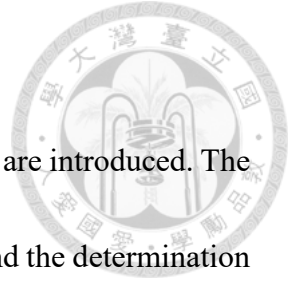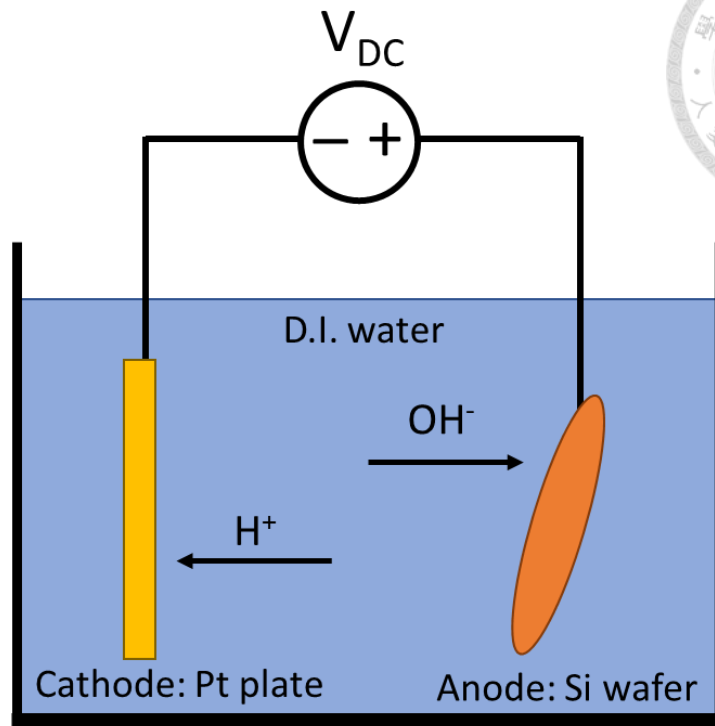
(b)

Figure 1-1. Schematic diagram of the anodization process. Silicon wafer is connected to anode and tilted in a certain angle while the platinum plate is connected to cathode.
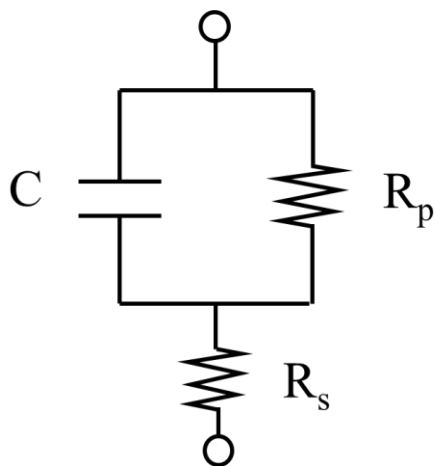
(a)   **(b)**
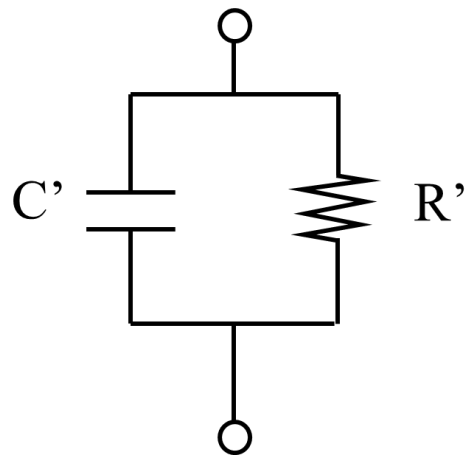
Figure 1-2. (a)The accurate circuit model and (b)the equivalent parallel model of the MIS TD.
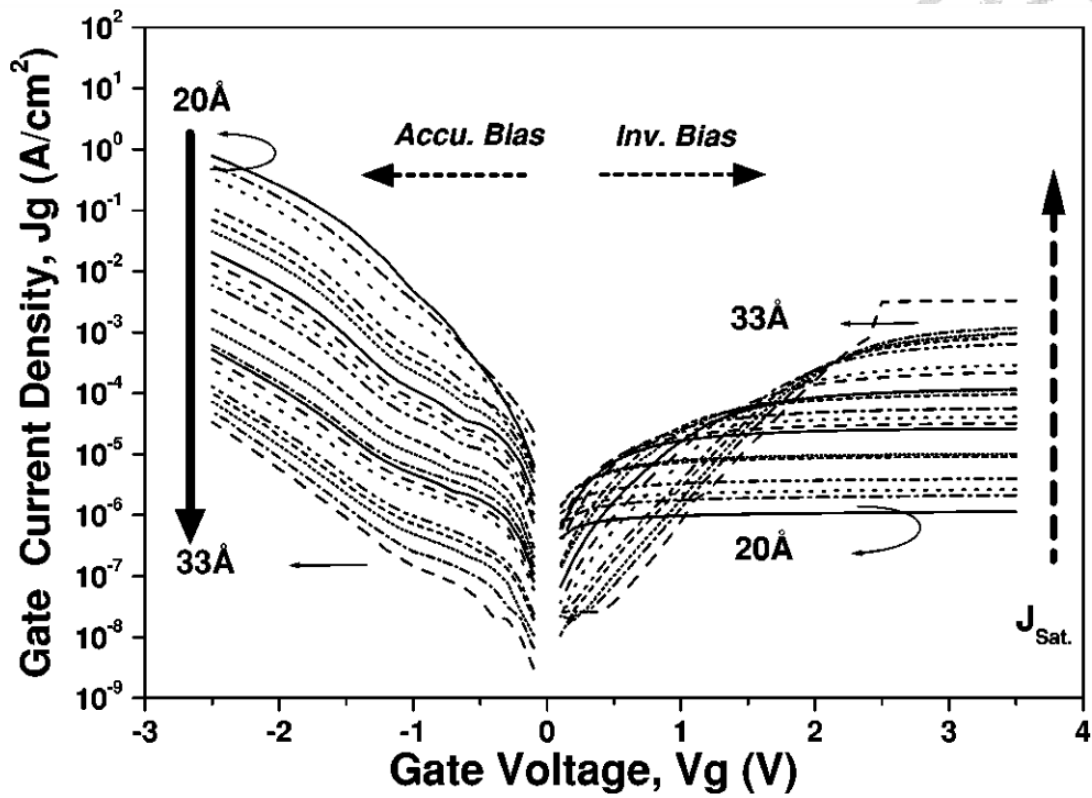
Figure 1-3. J_g-V_g curves of p-type substrate MOS devices with different oxide thickness (d_{ox}). It is observed that the current behavior in accumulation and inversion region had opposite tendency with d_{ox} [16].
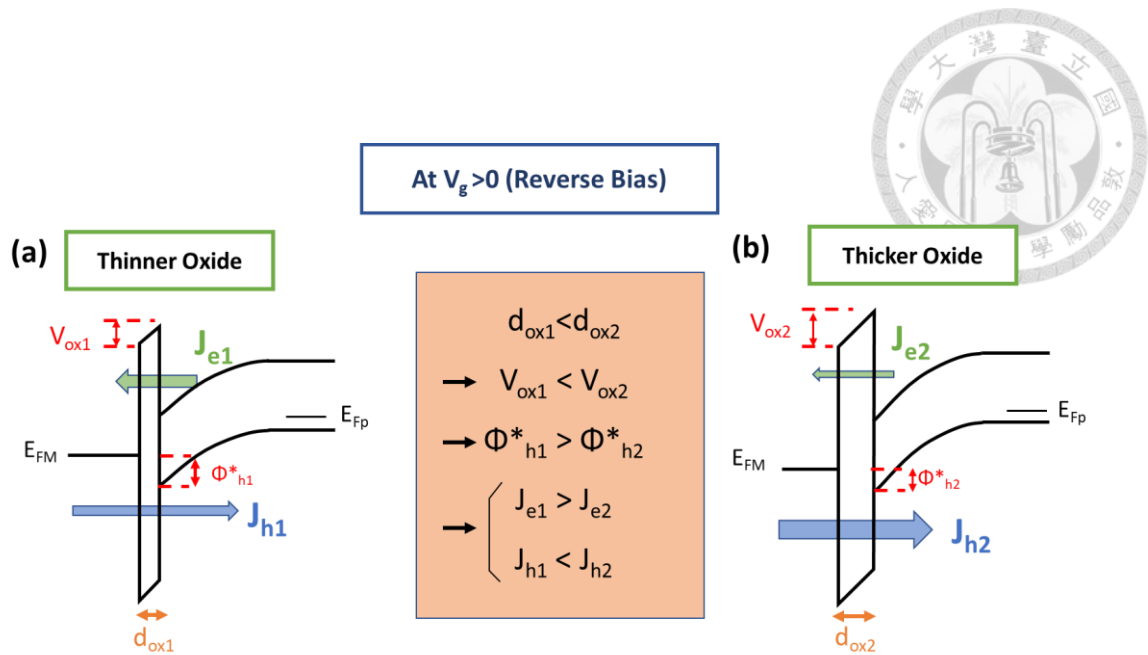
Figure 1-4. Schematic diagram of MISTD with (a)thinner oxide and (b)thicker oxide to explain the saturation current behavior by the SBH modulation.
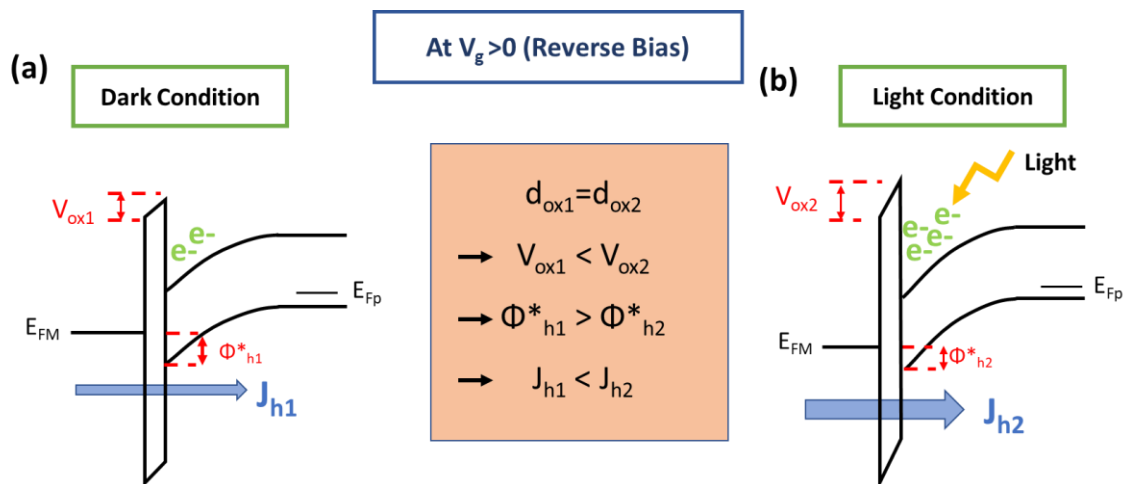
Figure 1-5. Schematic diagram of MISTD under (a)dark condition and (b)light condition to explain the current enhancement due to reduction in effective Schottky barrier height.
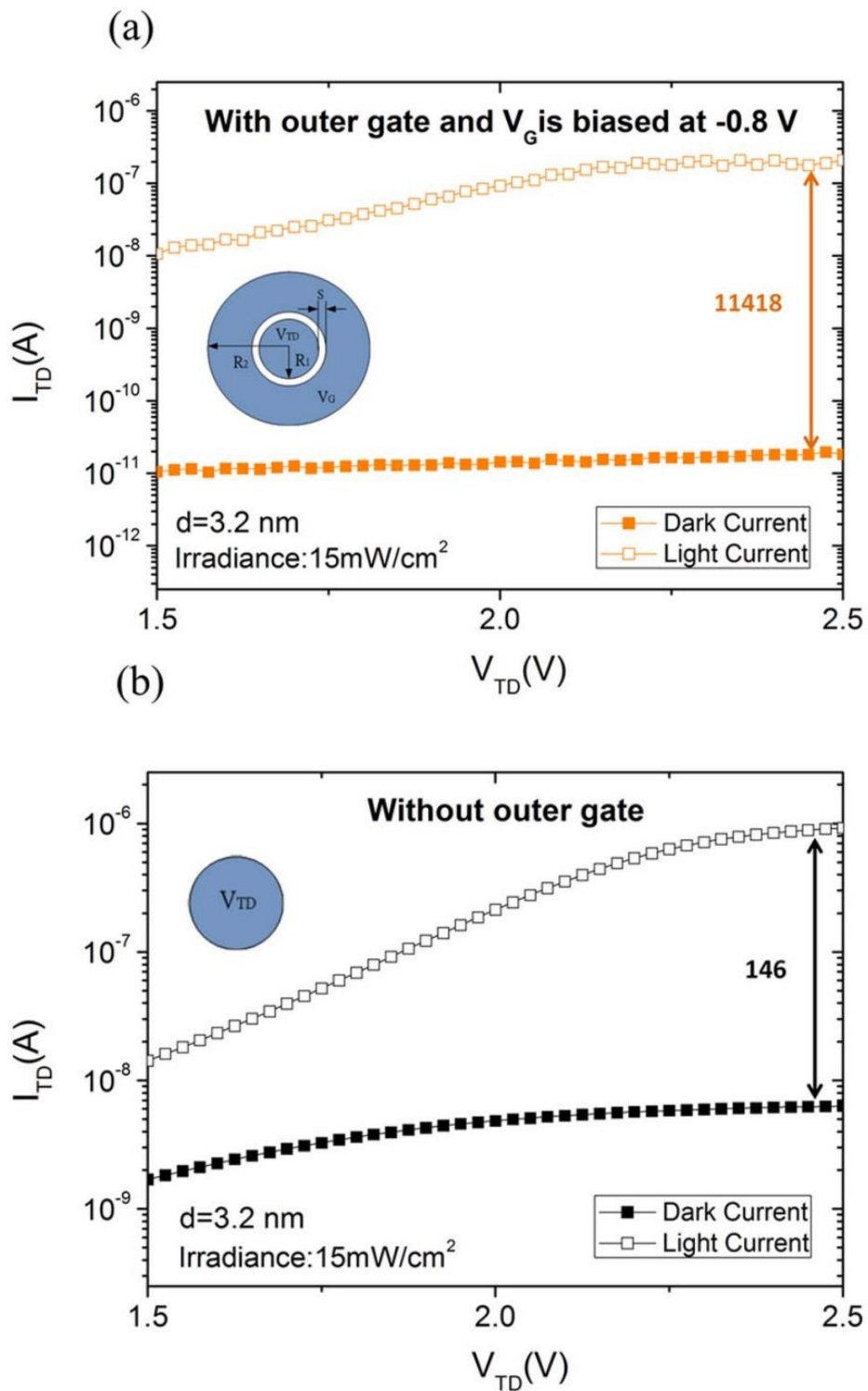
Figure 1-6. The current-voltage behavior of MISTD (a) with and (b) without additional outer gate. It is shown that photo response could be effectively enhanced by properly biasing V_G on the outer gate [20].

14
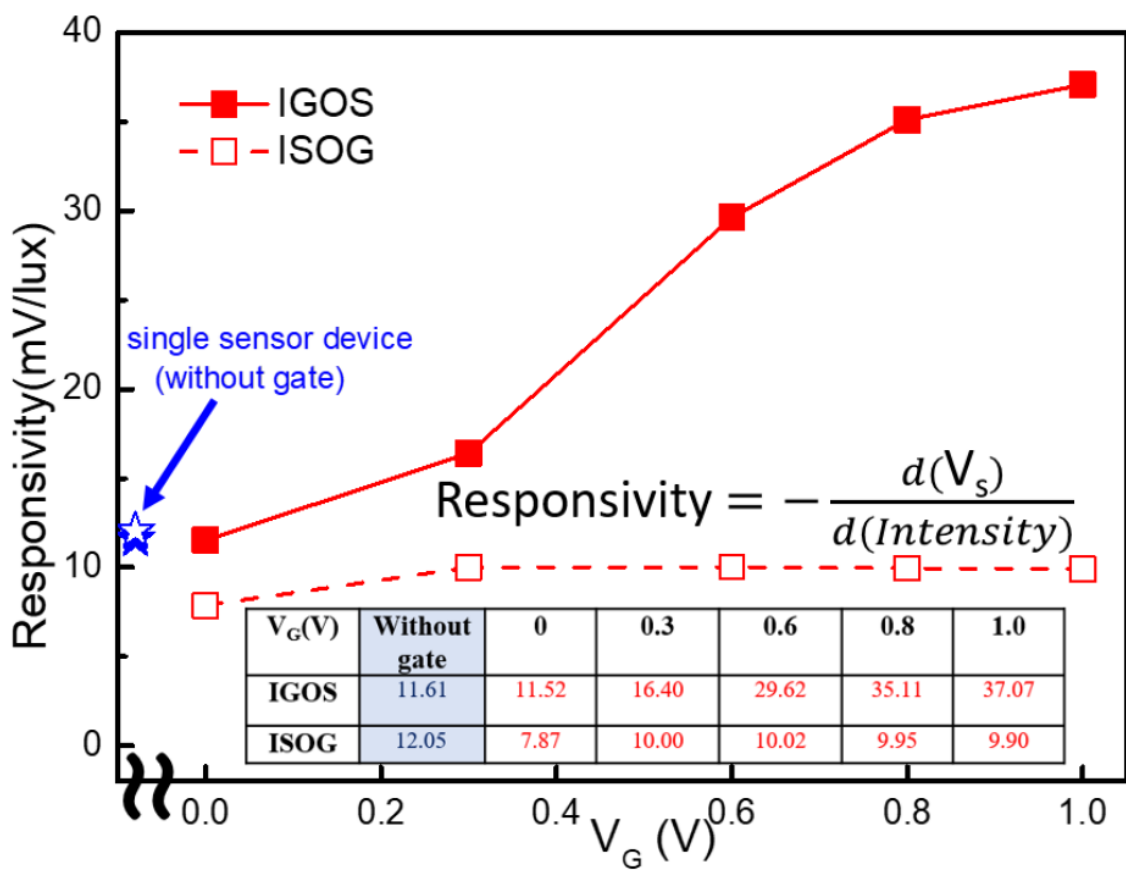
Figure 1-7. Responsivity versus gate voltage of ISOG and IGOS devices. It is observed that the responsivity of IGOS device is greatly better than the ISOG and single sensor device. [21]

Chapter 2
Characteristics of Al$_2$O$_3$ Passivated Metal-Insulator-Semiconductor (AOP-MIS) Devices

2-1   Introduction

In this chapter, we provids the experimental details of fabricating MIS and AOP-MIS devices used in this work in section 2-2. Then, the I-V and C-V characteristics of AOP-MIS devices are compared with MIS devices in section 2-3. Finally, the mechanism of how Al_2O_3 layer affects the device's performance is further discussed in the last section. It is observed that with the help of Al_2O_3 layer, the behaviors of both capacitance and current are changed significantly. The capacitance of the AOP-MIS devices becomes much higher than the MIS devices in the inversion region. Also, due to the enhancement of the local electric field by aluminum oxide layer, the saturation current is enlarged.

2-2   Experimental and Device Structure

The process flows of MIS and AOP-MIS devices are shown in Fig. 2-1. A 3-inch boron-doped 1-10 Ω-cm (100)-oriented p-type silicon wafer was used as the substrate. Firstly, the wafer went through standard Radio Corporation of America (RCA) clean. After the impurities and native oxide on the surface were removed, the wafer went through ANO process to grow high quality oxide. In this step, the wafer was tilted in order to make the thickness of oxide layer vary from 2.7 nm to 3.0 nm at room temperature. Then, rapid-thermal-annealing at 950°C for 15 seconds in N_2 ambient was carried out to repair defect in the oxide layer. Subsequently, a 200 nm Al film was deposited on the

17
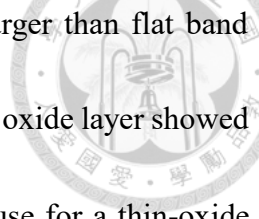
oxide layer by thermal evaporation. Afterwards, photolithography and wet etching were

carried out to define electrode area for the MIS devices. As for the AOP-MIS devices, the

same pattern was used to define electrode area. However, wet etching was conducted in

room temperature to slowly etch Al layer until it remained a thin film besides from the

electrode part. After that, the wafer was dipped into nitric acid solution for 3 minutes to

form Al_2O_3 layer. Finally, the photoresist was removed and the devices were done. The

schematic diagrams and the cross sections of MIS device and AOP-MIS device are shown

in Fig. 2-2. Compared to conventional MIS devices, there is an Al_2O_3 layer surrounding

the gate electrode and above the oxide layer in the region other than electrode area in

AOP-MIS devices.

2-3   C-V and I-V Characteristics

To compare how high-k layer affects MIS devices, the comparison of gate

capacitance versus gate voltage (C_G-V_G) curves and gate current versus gate voltage (I_G-

V_G) curves are discussed in this section.
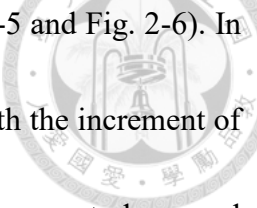
The C_G-V_G curves for MIS and AOP-MIS devices are shown in Fig. 2-3(a) and (b),

respectively. The I_G-V_G curves of them are shown in Fig. 2-4. In accumulation region,

the behavior of gate current is more related to the thickness of oxide layer. Therefore, it

is observed that with the similar thickness of oxide layer, gate capacitance and gate

current are similar for MIS devices and AOP-MIS devices. Nevertheless, the behavior

18

of two devices started to distinguish after the gate voltage was larger than flat band

voltage ($V_{FB} \approx$ -0.9V). For C_G-V_G curves, the MIS device with 2.7nm oxide layer showed

the effect of deep depletion as observed in previous studies. Because for a thin-oxide

device, the minority carrier was not sufficient, it had more tendency of having larger

depletion region and thus had more space charge to compensate the positive voltage.

Therefore, the depletion width increased with voltage, and the capacitance becomes

lower. However, for AOP device with similar oxide thickness, it seemed that the

minority carrier was more sufficient and thus could reach higher capacitance at low

frequency.

Aside from the differences of devices' performance shown in C_G-V_G curves, the

behavior of gate current in the depletion region and the inversion region also differed

accordingly. For MIS device, the current saturated after gate voltage approximately

larger than 0.7 V (Fig. 2-4). On the contrary, for AOP-MIS device, the gate current was

larger than MIS device in reverse bias. Besides, the gate current became greater as the

gate voltage increased, and it did not saturate even when the gate voltage reached 1V.

The phenomenon showed that unlike the MIS device, there was more minority carrier

able to respond, and thus had larger current. The detailed mechanism would be
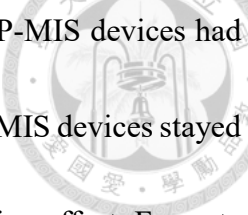
discussed in the next section.

Here, the measurements of C_G-V_G curves and I_G-V_G curves of both MIS and AOP-

MIS with different oxide thickness(d_{ox}) were also conducted (Fig. 2-5 and Fig. 2-6). In accumulation region, two kinds of devices had similar tendency. With the increment of the oxide thickness, both the gate capacitance and the leakage current decreased accordingly in this region. As for inversion region, with the increment of oxide thickness, the deep depletion behavior can be suppressed, and therefore the capacitance increased, which is shown in the C_G-V_G diagram in Fig. 2-5(a). However, the low frequency capacitance of the MIS devices with oxide thickness under 2.8nm is still lower than 25pF. On the contrary, for all AOP-MIS devices, it could maintain high capacitance with oxide thickness ranging from 2.7- 2.8 nm.

As for the behavior of the gate current (Fig. 2-6), MIS devices showed the phenomenon of saturation current overturn in the inversion region as expected. That is, the saturation of current happened earlier but the current would be lower for devices with thinner oxide. However, it would saturated under higher gate voltage and had higher value in inversion region for those with thicker oxide. In contrast to the MIS devices, the gate current purely increased with the thickness of oxide getting higher for AOP-MIS devices. In addition, the current did not saturate with oxide thickness of 2.7 nm. Also, with high-k layer, the performance of gate current can be enhanced under the same oxide as MIS devices.
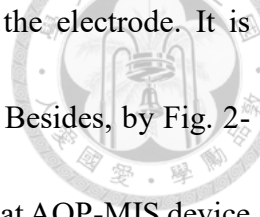
Fig. 2-7 further compared the characteristics of two kinds of devices. In Fig. 2-7(a),

it can be observed that under similar range of $C_{G@-2V}$, all of the AOP-MIS devices had high capacitance $C_{G@+1V}$ which was around 300 to 350 pF. However, MIS devices stayed at low value which was not larger than 30pF due to the deep depletion effect. For gate current (Fig.2-7(b)), the relation between current in saturation region and in accumulation region is represented. With $I_{G@-2V}$ in the range of 0 to 1000 nA of MIS showed the saturation current overturn behavior. However, for AOP-MIS devices, it is shown that $I_{G@+1V}$ purely decreased with oxide thickness. Also, the saturation current of AOP- MIS was larger than MIS device under the similar range of $I_{G@-2V}$ which also represented that they are under similar range of oxide thickness. With $I_{G@-2V}$ around 430 nA, the saturation current of AOP-MIS device can up to about 4 times larger than MIS device. Moreover, when the oxide layer becomes even thinner, the gate current $I_{G@+1V}$ could reach about 33 nA.

2-4   Mechanism Discussion

To further understand the effect of AOP layer, TCAD simulation was conducted. The structures of MIS device and AOP-MIS device used in simulation are shown in Fig. 2-8. It is noted that the thickness of SiO_2 layer (d_{ox}) and Al_2O_3 layer (d_{AOP}) are 30Å and 10nm, respectively. Also, models of self-consistent direct tunneling in all the forms [22], Shockley–Read–Hall recombination [23]-[24], Auger recombination [25], and Bohm quantum potential accounting for the quantum confinement effect [26] are used here. Fig.

21

2-9 displays the results of simulated electric field at the edge of the electrode. It is observed that the fringing field of AOP-MIS device extends further. Besides, by Fig. 2-10, which shows the cutline of electric field near surface, it is found that AOP-MIS device has higher fringing field outside the electrode than MIS device. Therefore, it is supposed that with the existence of AOP layer, the fringing field would be enhanced and extended to further region.

Also, SBH modulation theory is introduced to explained the difference of current behavior between MIS and AOP-MIS device here. By SBH modulation theory, the saturation current is strongly related to the tunneling effect happening at the edge of device. The behavior of current is similar to a Schottky diode. The current can be written as

$$J_h \propto \exp(-\frac{e\phi_B}{k_B T}) \ , \qquad\qquad (2\text{-}1)$$

where ϕ_B is the Schottky barrier height, k is the Boltzmann constant and T is the temperature. With a layer of high-k surrounding the device edge, the edge electric field (E) would be enhanced. Therefore, there is a larger potential drop on oxide layer (V_{ox2}) than that of the MIS device (V_{ox1}). The band diagram is depicted in Fig. 2-11. With the help of high-k layer, the Schottky barrier height at the edge at which the majority hole carrier faced decreased, which means there are more holes able to tunneling through the oxide layer. As a result, according to Eq. (2-1), the hole current J_h would become larger.

22

This leads to the result that the total current of AOP-MIS device could be higher than MIS device with the same oxide layer.

2-5   Summary

In this chapter, we proposed and fabricated Al_2O_3 passivated (AOP) MIS devices. Two electrical characteristics of C_G-V_G and I_G-V_G curves of it was shown and compared with traditional MIS devices. From these data, we found that the deep depletion behavior would be suppressed with the help of the Al_2O_3 layer, and the gate capacitance therefore can reach higher value in inversion region. The mechanism that due to the lowered Schottky barrier height in AOP-MIS devices, more carriers are able to tunneling through and injecting into substrate was also proposed.
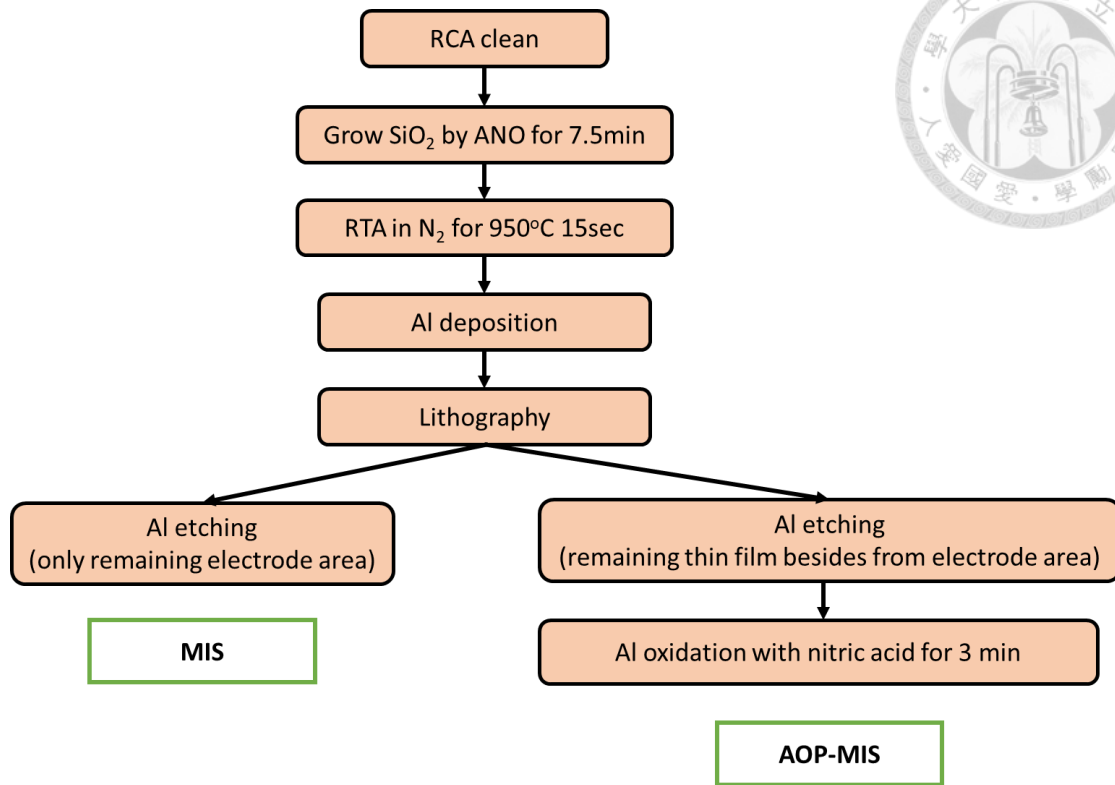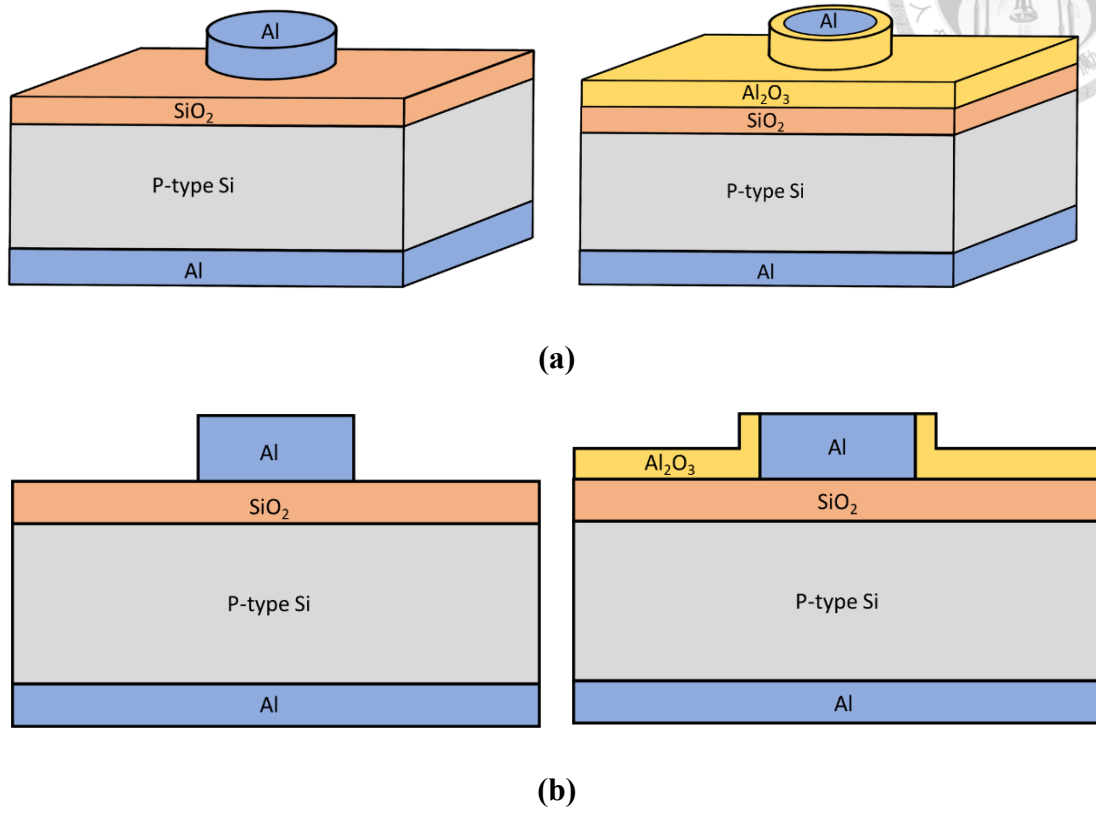
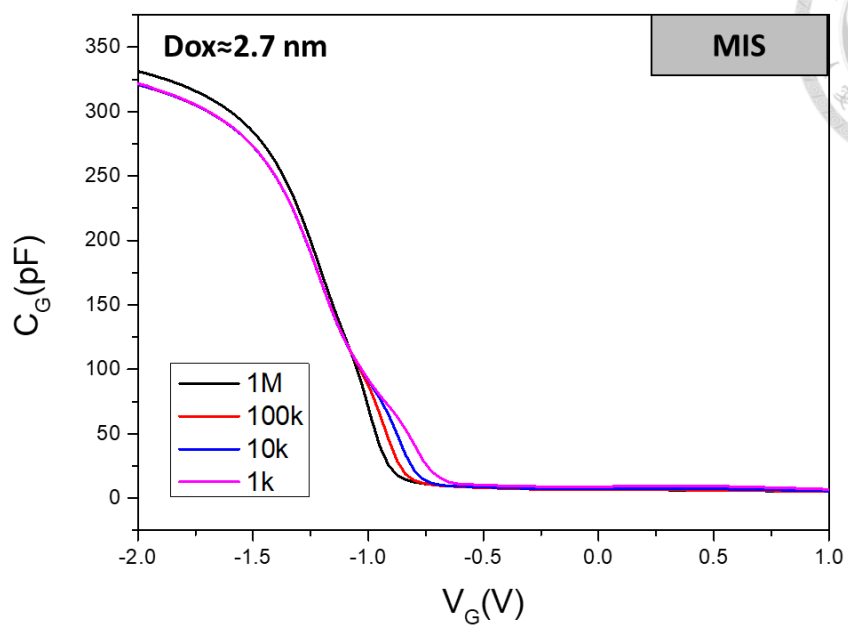**Figure 2-1. The experimental process flow.**
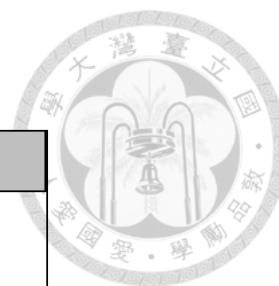
Figure 2-2. (a) Schematic diagram of the MIS device(left) and AOP-MIS device(right) and (b) cross sections of them.

(a)
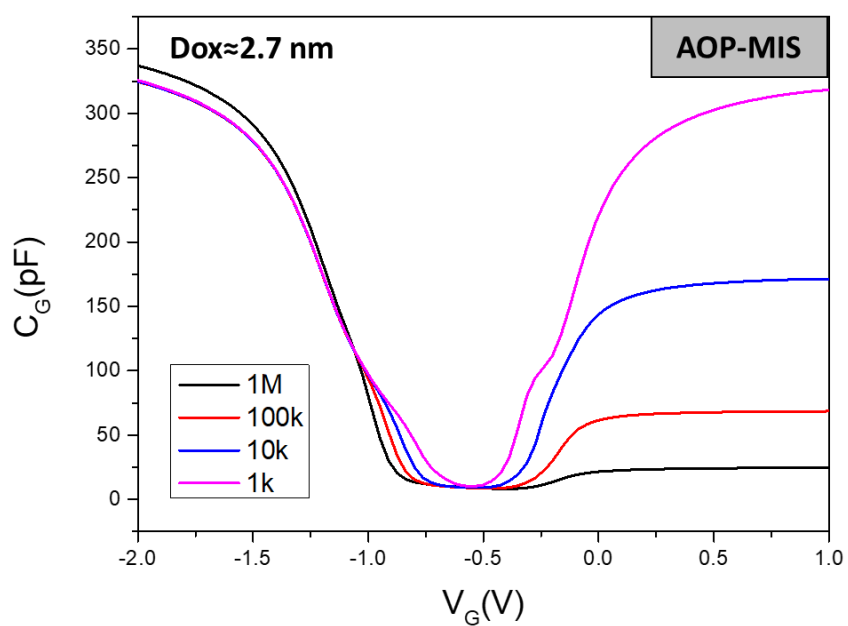
(b)

Figure 2-3. The comparison of the C_G-V_G curves of (a) MIS device and (b) AOP-MIS device with 2.7nm oxide layer.
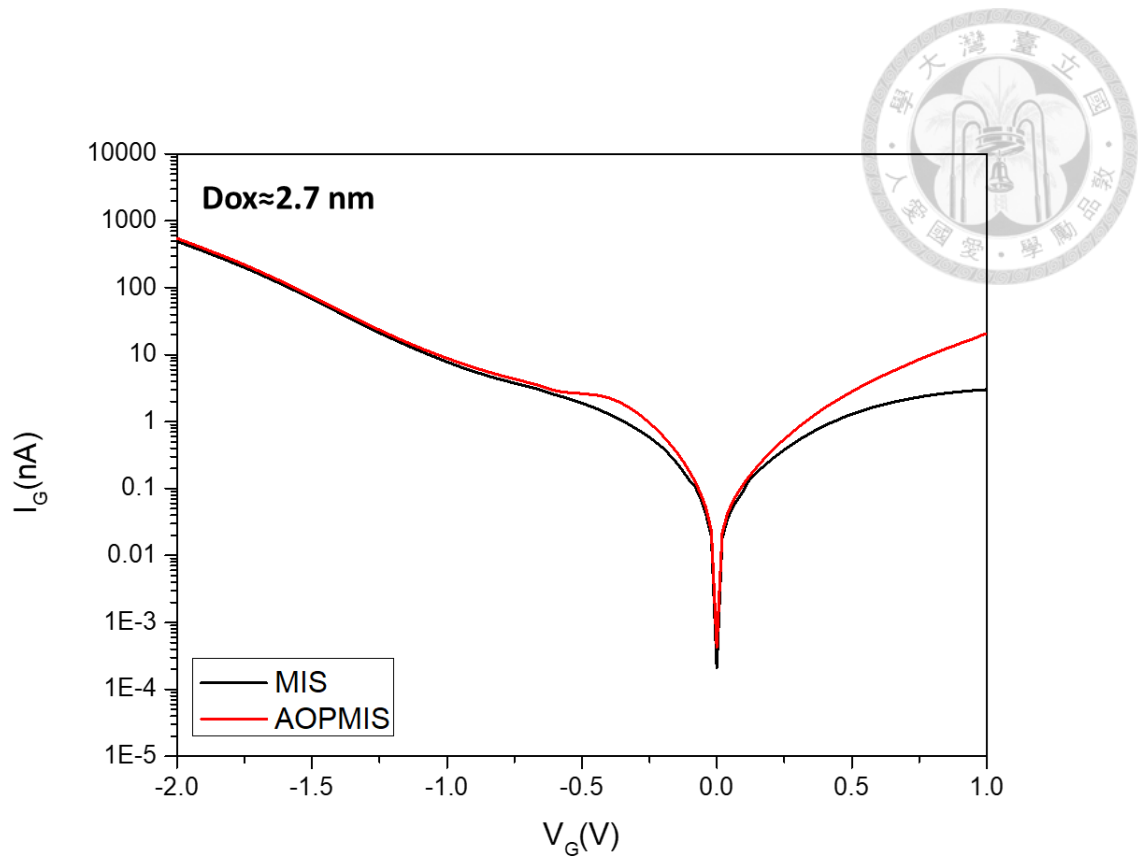
Figure 2-4. The comparison of the I_G-V_G curves of MIS device (black line) and AOP-MIS device (red line).
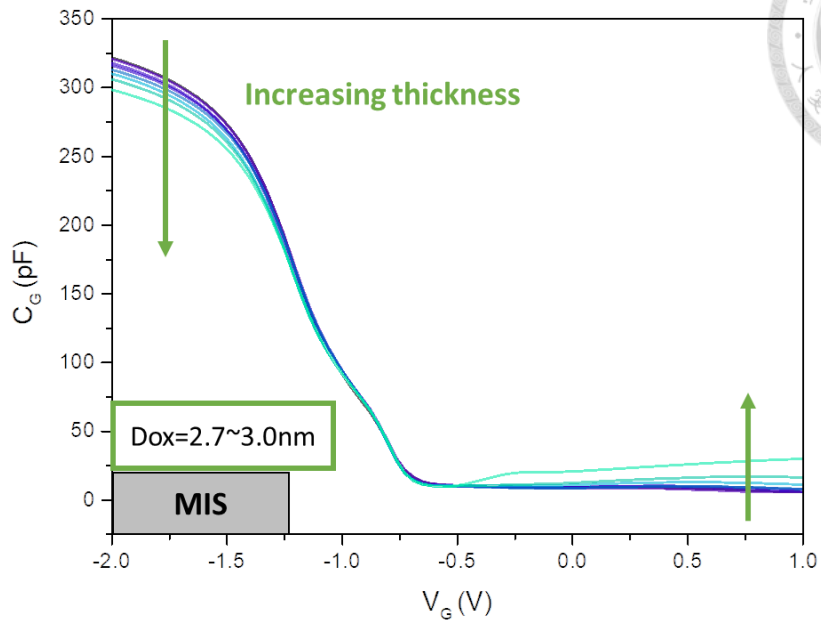
(a)
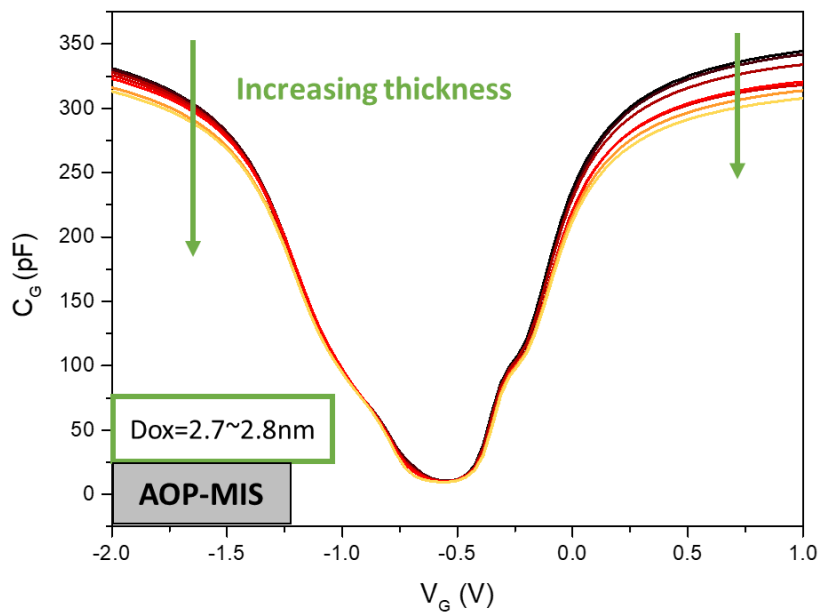
(b)

Figure 2-5. The comparison of the C_G-V_G curves under frequency of 1kHz of (a) MIS devices and (b) AOP-MIS devices under different oxide thickness.

28
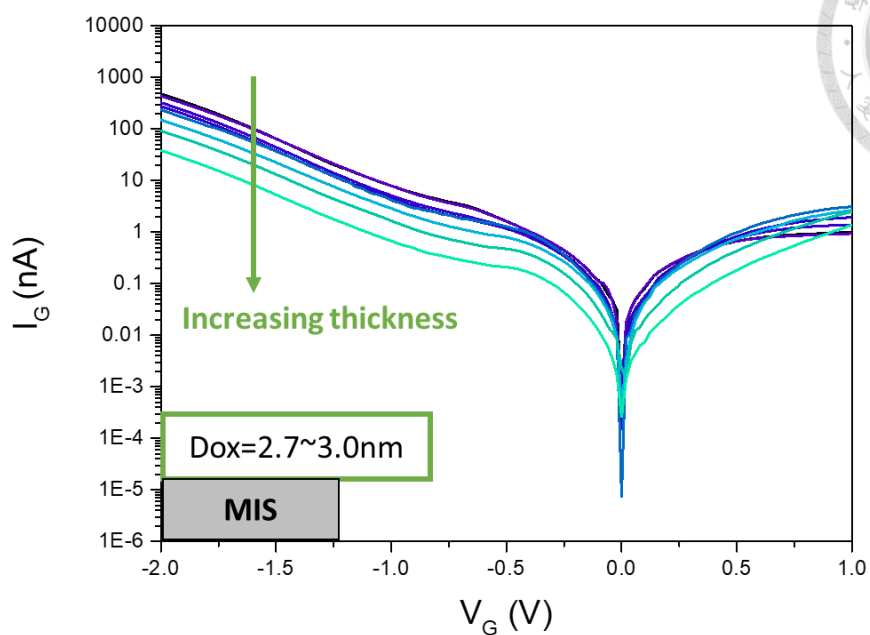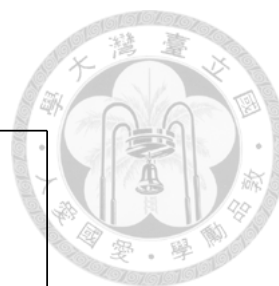
(a)
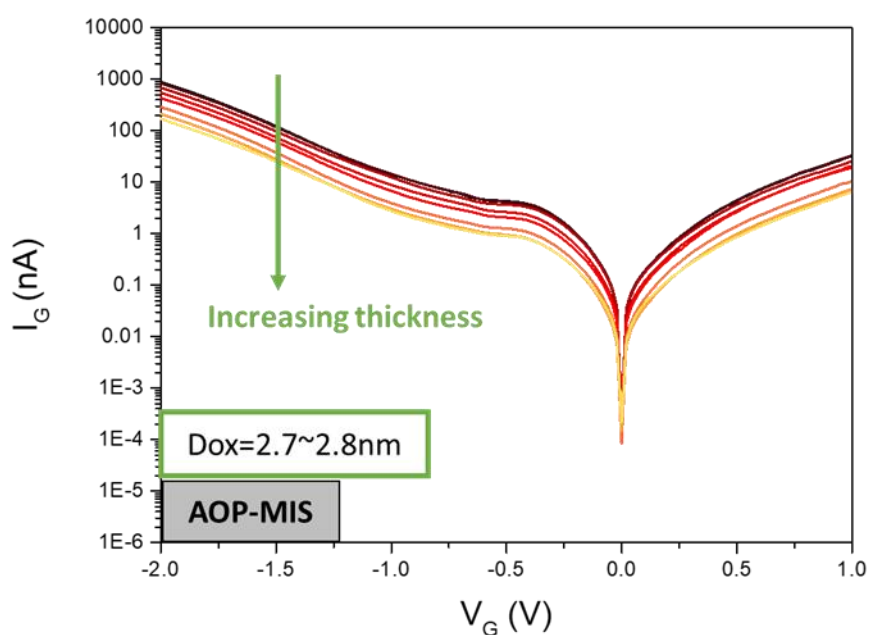
(b)

Figure 2-6. The comparison of the I_G-V_G curves of (a) MIS devices and (b) AOP-MIS

devices under different oxide thickness.

29
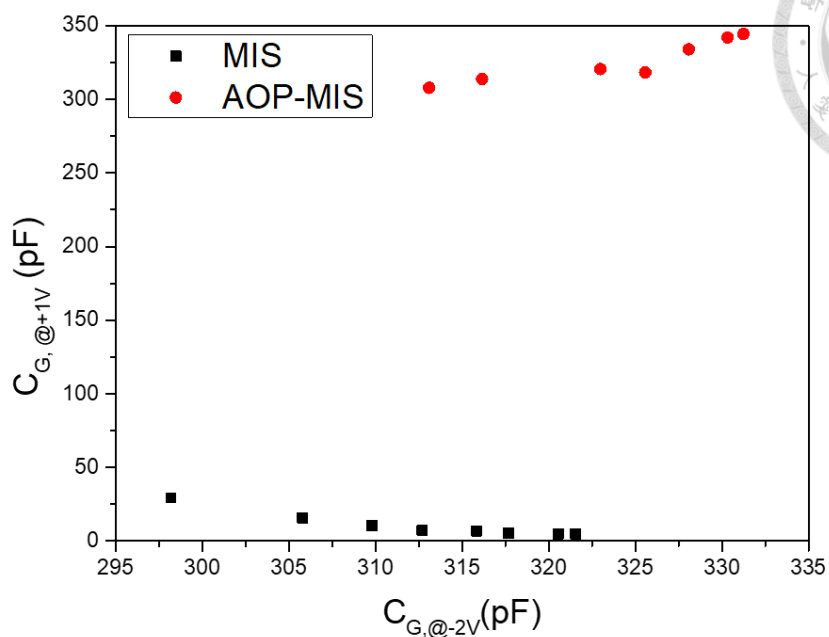
(a)
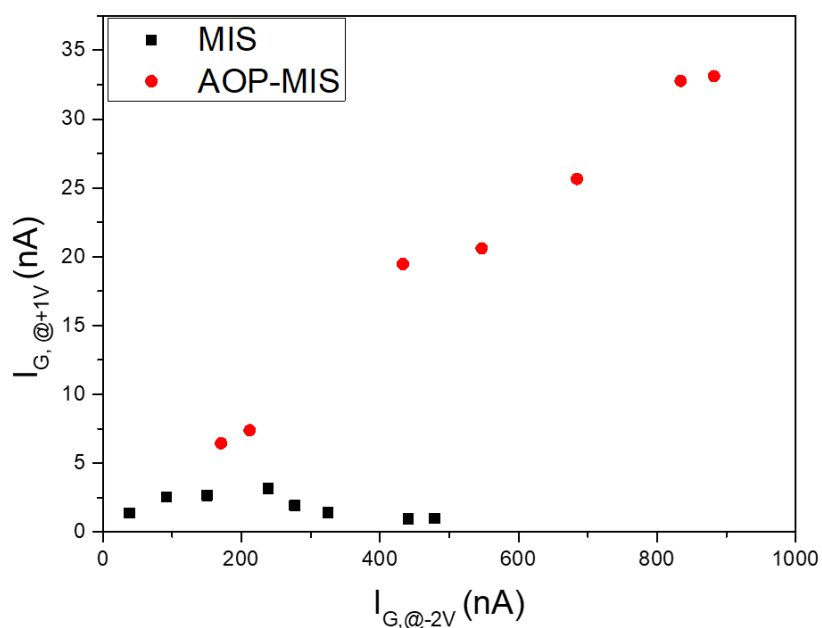
(b)

Figure 2-7. The comparison of the (a) $C_{G, @+1V}$ versus $C_{G, @-2V}$ under frequency of

1kHz and (b) $I_{G, @+1V}$ versus $I_{G, @-2V}$ between MIS devices and AOP-MIS devices.
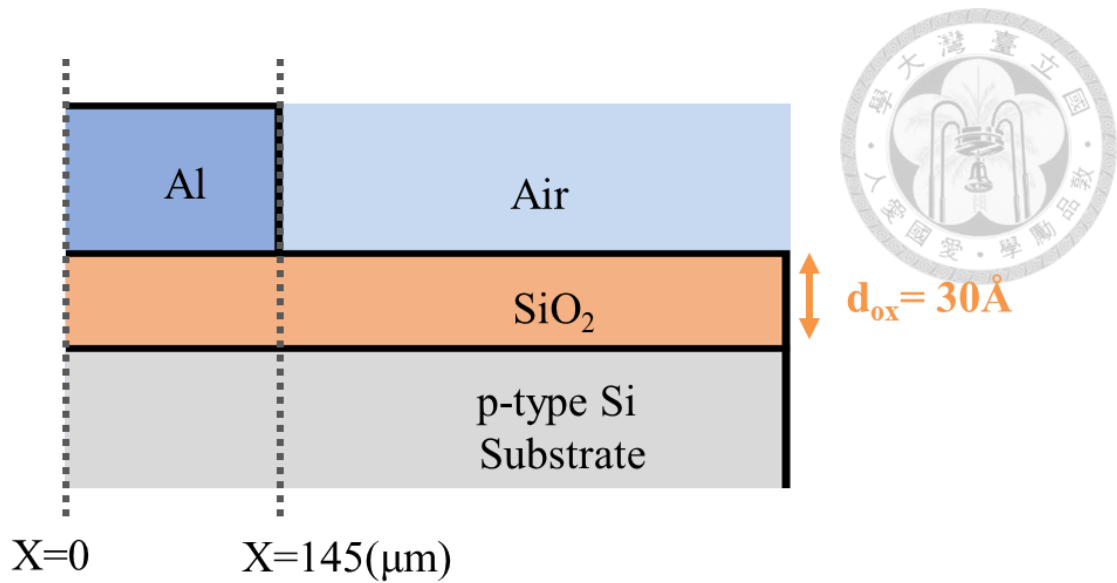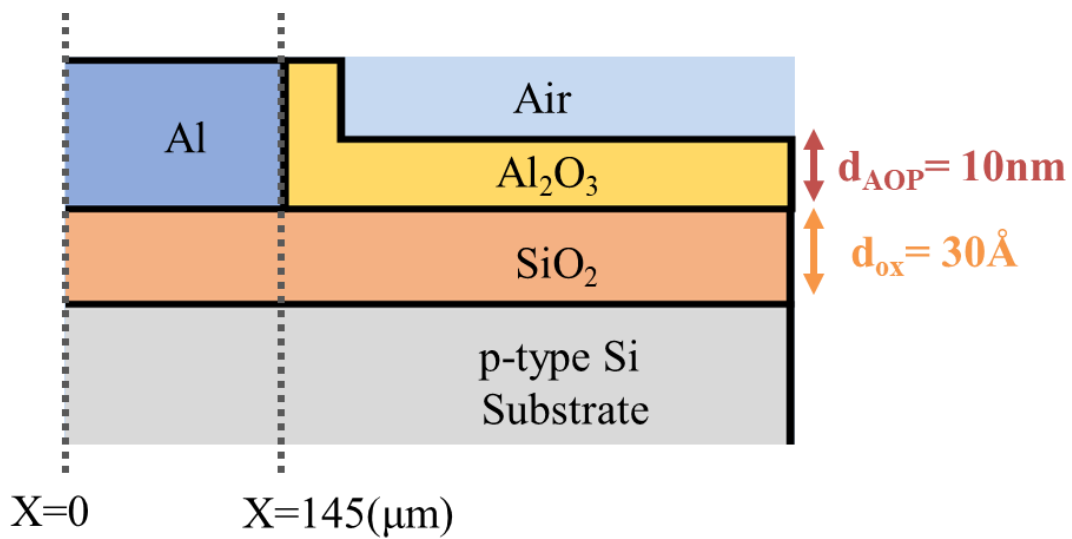
Figure 2-8. The schematic diagram of structure of (a) MIS and (b) AOP-MIS device used in TCAD simulation. The thickness of SiO$_2$ layer (d$_{ox}$) and Al$_2$O$_3$ layer (d$_{AOP}$) are 30Å and 10nm, respectively.
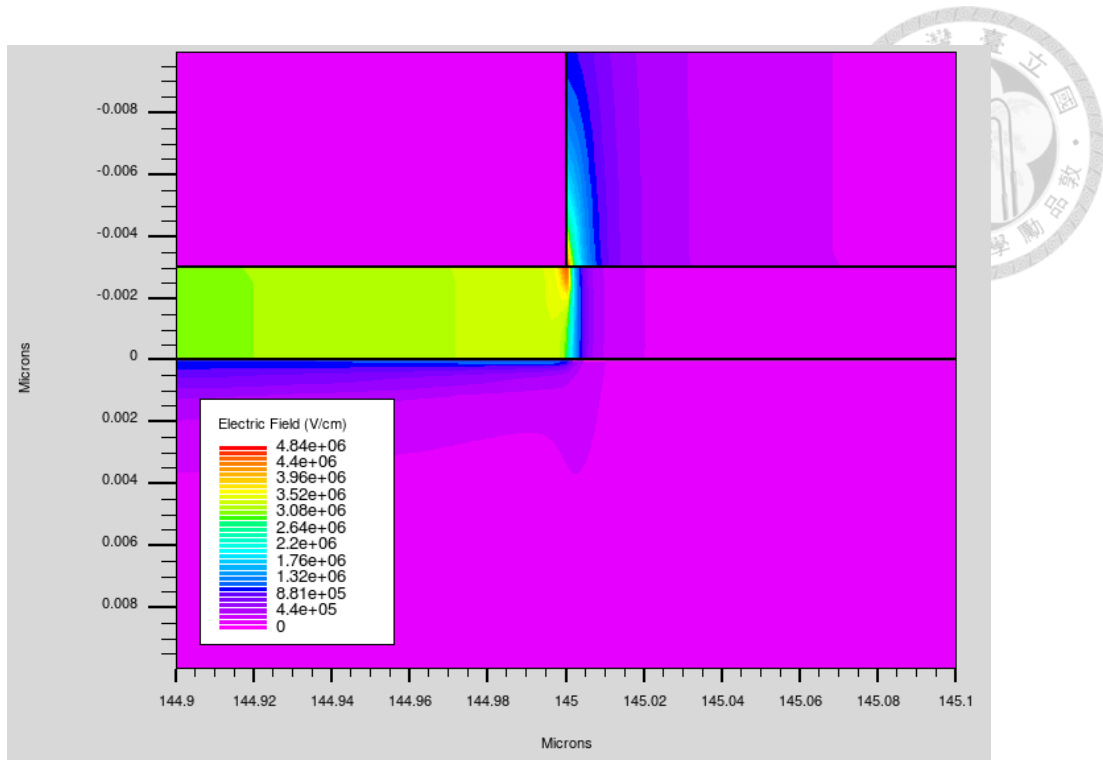
(a)
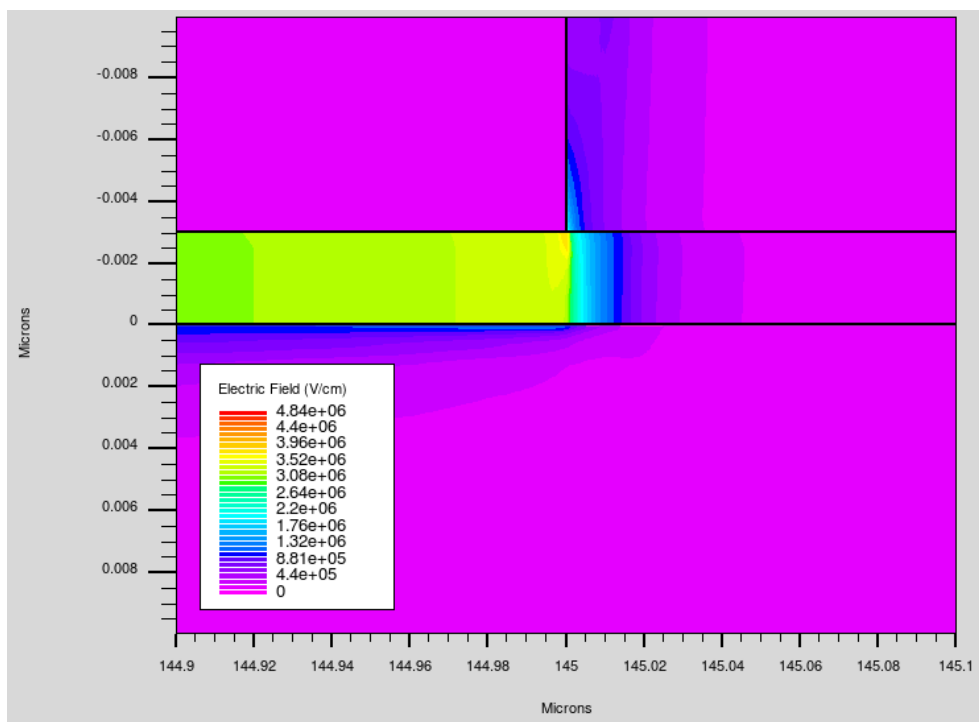
(b)

Figure 2-9. The TCAD simulation results of electric field of (a) MIS device and (b)

AOP-MIS device under V_G= 1V.
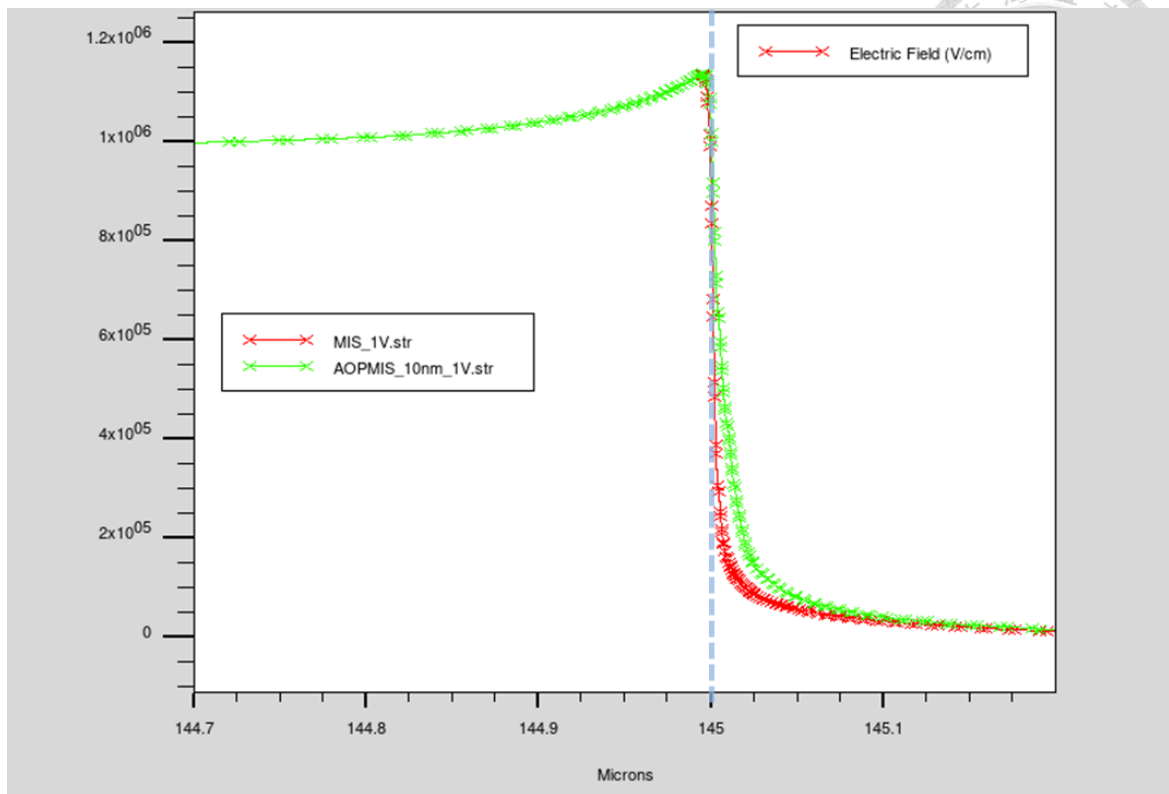
Figure 2-10. Cutline of simulated electric field near the surface (Y= 1E-5µm) of MIS (red line) and AOP-MIS device (green line.) It is found that the AOP-MIS device has larger fringing field than MIS device.
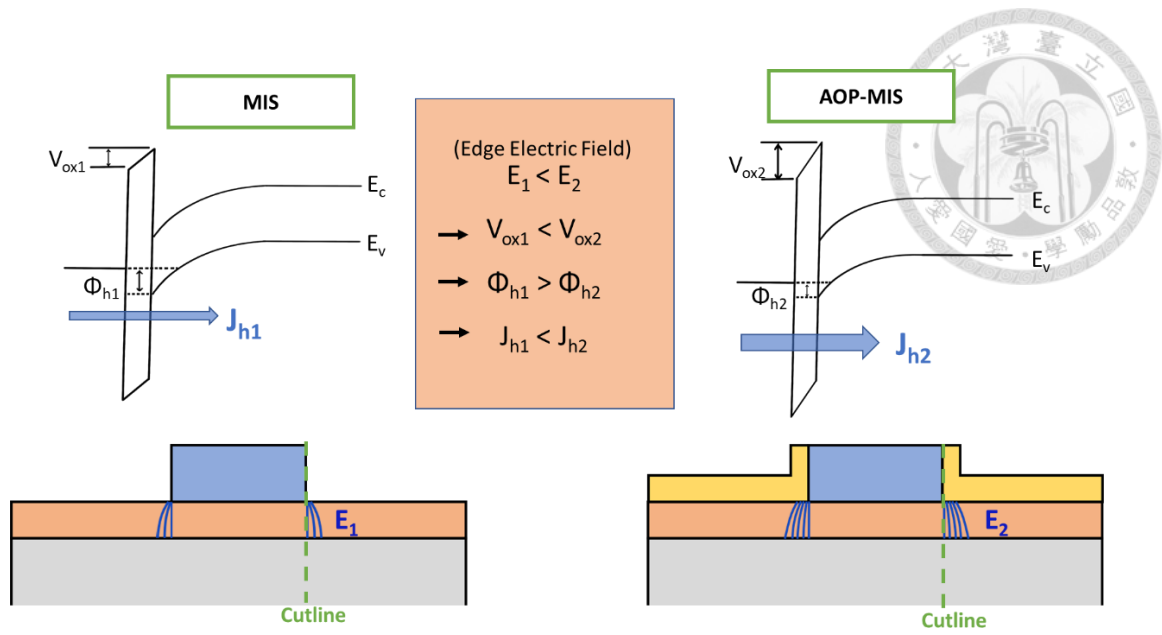
Figure 2-11. Band Diagrams and schematic diagrams of electric field in the SiO₂ layer of MIS device and AOP-MIS devices at reverse bias.

Chapter 3
Application of Al$_2$O$_3$ Passivated Metal-Insulator-Semiconductor (AOP-MIS) Devices as Light Sensors

3-1 Introduction

In this chapter, the effect of light on MIS and AOP-MIS was studied. All devices were fabricated under the same process introduced in Chapter. 2. The oxide thickness of the devices are ranging from 2.7 nm to 3.0 nm. In section 3-2, representative devices for each of two kinds of devices were chosen for comparison. The result of C_G-V_G and I_G-V_G characteristics under different light illuminance conditions were discussed. Furthermore, in section 3-3, the mechanism of light current under different gate voltage was proposed. Finally, in the last section, we compared some representative parameters of light sensing performance of MIS device and AOP-MIS device. We find that with the help of the aluminum oxide layer, which enhances the local electric field at the edge, the AOP-MIS devices can gather more excess carrier generated by light at the edge of the device. Hence, they were more sensitive to light, and hence showed better performance. Not only open circuit voltage but also short circuit current has larger difference under different light illuminance.

3-2 Overview of I-V and C-V Characteristics

The measurements of gate current and capacitance with different illuminance of light casting on both MIS and AOP-MIS devices were conducted. Fig. 3-1 shows the comparison of the C_G-V_G curves of (a) MIS device and (b) AOP-MIS devices with 2.7nm oxide layer under different light illuminance. Also, the corresponding change in the gate

36
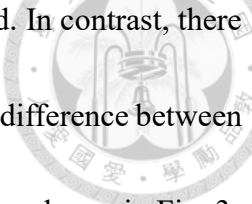
current is presented in Fig. 3-3 as well. According to Fig. 3-1, it is observed that under

dark condition, the C_G-V_G curves of AOP-MIS device did not show the tendency of deep

depletion as the discussion in the last chapter. When there is a light source provided, the

light would intrigue the generation of electron-hole pair in the substrate. Thus, it makes

the device more like to catch up the voltage response, which leads to the increasement of

capacitance. The difference of capacitance under dark and light was also calculated. It is

defined as below.

$$C_{G, diff} = C_{G, light} - C_{G, dark} \tag{3-1}$$

The result of $C_{G, diff}$ - V_G curves is shown in Fig. 3-2. Compared to purely slight change

in capacitance of the MIS device, the AOP-MIS device had higher sensitivity to

illuminance change. The maximum difference of capacitance of AOP-MIS device was up

to more than 110pF, while for MIS device, it could not even reach 10pF. Although the

reason of the existence of two peaks of capacitance with 1kHz-frequency in Fig.3-2 (b)

was not fully studied and analyzed yet, it cannot be ignored the possibility of using the

AOP-MIS device as light sensor.

As for gate current, both MIS device and AOP-MIS devices showed the behavior of

response to light. The current was enhanced due to the generation of excess carriers due

to light. With the illuminance of light increased, the current was enlarged accordingly.

However, for MIS devices, there is a tendency that its light current would saturated and

37

was difficult to reach higher value even the intensity of light increased. In contrast, there is more room for the light current of AOP-MIS device to increase. The difference between the light current and the dark current ($I_{G,diff}$) of two kinds of devices are shown in Fig. 3-3(b). It is observed that the $I_{G,diff}$ of AOP-MIS device could be more than twice as large as $I_{G,diff}$ of MIS device when $V_G= +1V$.

3-3 Mechanism Discussions of MIS Devices and AOP-MIS Devices

In this section, we would compare the mechanism of light current of two devices. The comparison of $I_{G, diff}$-V_G curves and $C_{G, diff}$-V_G are shown in Fig. 3-4. It seemed that based on the behavior of current and capacitance, we can divide it into three different regions, which is $V_G< V_{FB}$ ($\approx$-0.9V), $V_{FB}< V_G< 0$, and $V_G> 0$ as Region 1, 2, and 3, respectively.

In region 1, the gate voltage was more negative than flat band voltage, which represented that the device was in accumulation region. In this region, since the negative bias, the current is mostly contributed by electron carriers flow along the electric field. A huge amount of electron would inject into the substrate. The schematic diagram was shown in Fig. 3-5. The current was determined by the thickness of oxide layer, and the effect of light was negligible. Hence, there was no obvious difference in two devices.

As for region 2, which is $V_{FB}< V_G< 0$, the devices were in depletion region. Although, the gate bias is still negative, which therefore makes electron flowing from gate to the

38
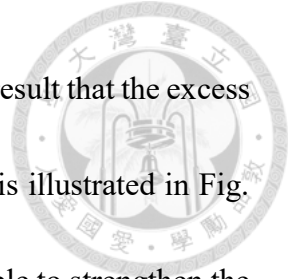
substrate, the surface electric field was flipped over here. It led to the result that the excess carriers generated by the light flow in the opposite direction, which is illustrated in Fig. 3-6. Similar to the discussions in the section 2-3, the Al_2O_3 layer is able to strengthen the electric field near the edge of device. Therefore, the ability to gathering excess carriers is better than MIS device. That is, the difference current $I_{G,diff}$ could become larger as the result shown in Fig. 3-4
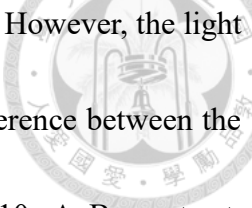
In the last region that $V_G > 0$, the direction of electric field caused by gate voltage is already overturn. The main electron flow is now overturn into the direction from substrate to metal. Moreover, the current flow at the edge of device is dominant now. The according schematic diagrams are shown in Figs. 3-7 (a) and (b), which stand for MIS and AOP-MIS devices, respectively. Furthermore, in this region, the built-in electric field at the edge is also from metal to substrate as region 2. Due to this electric field, the excess carriers cause an additional carrier flow, which is from substrate to metal for electron. Since the edge field becomes much greater than region 2, the influence of it hence becomes more obvious. That is, the difference current $I_{G,diff}$ is larger in this region for both MIS and AOP-MIS devices as shown in Fig. 3-4. Also, under the influence of the existence of Al_2O_3 layer, the edge electric field can be strengthened. This once again leads to the result of the value of $I_{G,diff}$ much larger than MIS device.

3-4 Representative Parameters of Light Sensing Performance

Eight different devices with different thickness of oxide layer for both MIS and AOP-MIS devices were fabricated. The oxide thickness of these devices is ranging from 2.7 nm to 3.0 nm. Then, we conducted a series of measurement on these devices, such as open circuit voltage (V_{oc}), short circuit current (I_{sc}), and their corresponding capacitances under different light intensities. The results are concluded as follows.

In Fig. 3-8, the comparison of open circuit voltage (V_{oc}) versus illuminance of MIS and AOP-MIS devices were presented. It is noted that the definition of open circuit voltage is the gate voltage where the gate current is zero at that time. From this figure, it is shown that although under weak light, there is no big difference can be observed. However, when the light intensity is increased, the response of devices seemed to differ. For MIS devices, the open circuit voltage had the tendency to saturate, and the difference between V_{oc} under light of 3.9 lux and 7.8 lux was less than 1mV. In contrast, the AOP-MIS did not saturate, but could reach higher value of V_{OC} under 3.9 lux and 7.8 lux. The difference between V_{oc} under light of 3.9 lux and 7.8 lux was 4 mV, which showed that AOP-MIS devices has better sensitivity of light change.
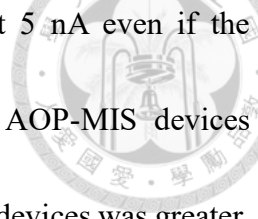
Also, the results of short circuit current (I_{sc}) reacting to the change of light illuminance of MIS and AOP-MIS devices were depicted in Fig. 3-9. The short circuit current was defined as the gate current under $V_G = 0$ V. It is observed that although under

condition of illuminance= 0.6 lux, I_{sc} of MIS device can reach 61 pA. However, the light

current started saturating when the light intensity increased. The difference between the

mean value of I_{SC} under light of 0.6 lux and 7.8 lux was not larger than 10 pA. By contrast,

for AOP-MIS devices, the difference between the mean value of I_{SC} was up to about 200

pA. Also, the response of I_{SC} to light intensity of AOP-MIS devices seemed to be more

linear than MIS devices, which indicated that AOP-MIS structure is a better choice for a

light sensor.

The change of gate capacitance at low frequency of 1kHz under similar conditions

were also measured and presented in Fig. 3-10. It is shown that under dark condition

(illuminance= 0 lux), the initial value of gate capacitance of AOP-MIS devices was higher

than that of MIS devices. Furthermore, under higher light intensity conditions, the

behavior of saturation of MIS devices can be observed again here. From the difference of

capacitance versus illuminance curves (Fig. 3-10(b)), it was observed that the mean value

of $C_{G, diff}$ was only 16 pF under light illuminance= 7.6 lux for MIS devices. However, for

AOP-MIS devices, the mean value of $C_{G, diff}$ was about 64 pF under the same condition,

which was four times larger than MIS devices.

Finally, the measurement of gate current in inversion region was conducted, and the

difference of current between light and dark was also calculated. Here, the gate voltage

of 1V was chosen. The results were shown in Fig. 3-11. From Fig. 3-11(a), it can be seen

that the gate current basically saturated and confined under about 5 nA even if the illuminance reaches 7.6 lux for MIS devices. Nevertheless, the AOP-MIS devices increase with the light intensity. Although the variation of AOP- MIS devices was greater, all of them could have larger value of gate current than MIS devices. In addition, it is noticed from Fig. 3-11(b) that the difference of light and dark current is close to a linear dependency on light illuminance for AOP-MIS devices, and the maximum difference could up to 17 nA, which is four times larger than MIS devices.

3-5 Summary

In this chapter, we examined the characteristics of devices' performance under light. Both I_G-V_G and C_G-V_G curves were explored. It is observed that after the light increases large enough, the current and capacitance would nearly become saturated for MIS devices. However, for AOP-MIS devices, the current would not saturate but could still increase as light intensity becomes higher. The mechanism that the Al_2O_3 layer can enhance local electric field at the edge was used to explain the higher sensitivity here again. With higher electric field, the ability to gather excess carrier is enhanced; therefore, AOP-MIS devices have higher light current than MIS devices. Finally, we examined V_{oc} and I_{sc} to find the ability of light sensing. The difference of I_{SC} between light (illuminance= 7.8 lux) and dark of AOP-MIS devices could reach 305 nA which is more than 3 times larger than that

of MIS devices. Also, at inversion region at $V_G = 1$ V, the $I_{G,diff}$ of AOP-MIS devices was four times higher than that of MIS devices.
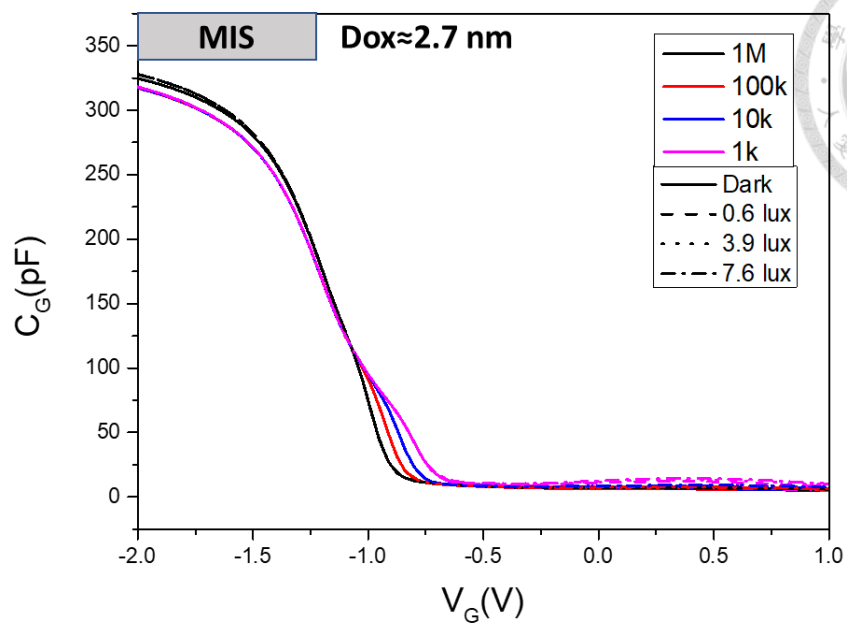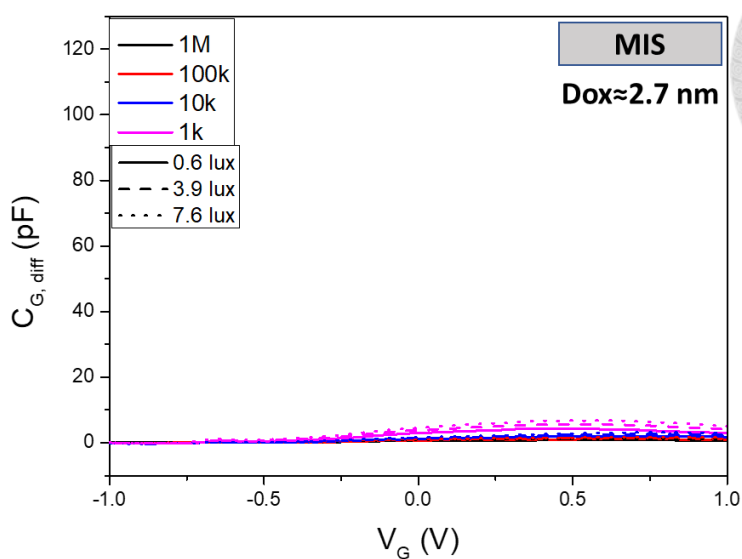
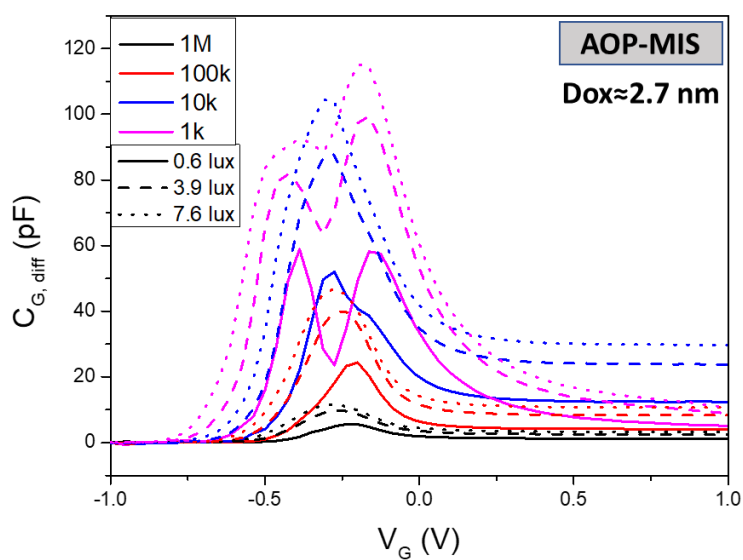**(a)**
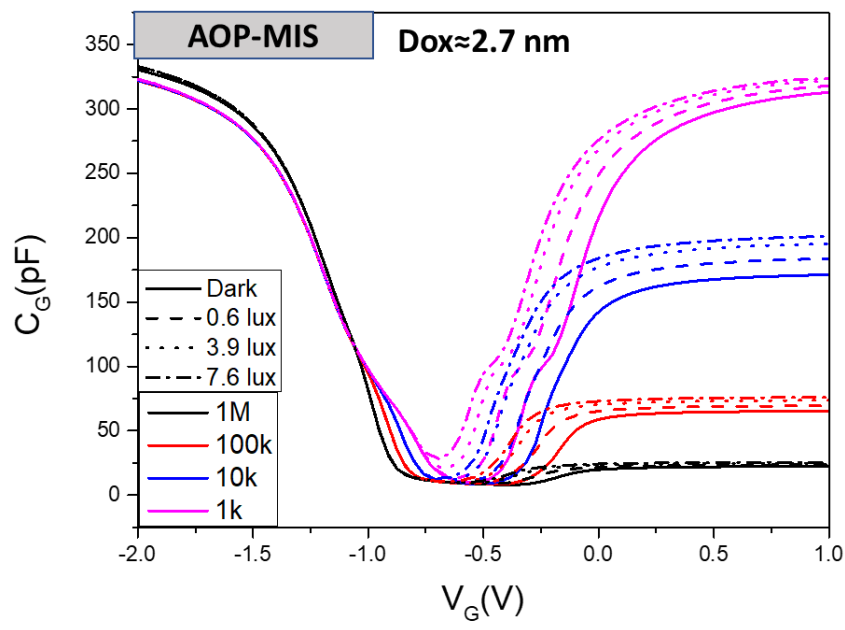
(b)

Figure 3-1. The comparison of the C_G-V_G curves of (a) MIS device and (b) AOP-MIS

device with 2.7nm oxide layer under different light illuminance (red: 0.6lux, blue:

3.9lux, pink: 7.6lux.)

(a)

(b)

Figure 3-2. The comparison of the difference of capacitance versus gate voltage ($C_{G,diff}$-V_G curves) of (a) MIS device and (b) AOP-MIS device with 2.7nm oxide layer under different 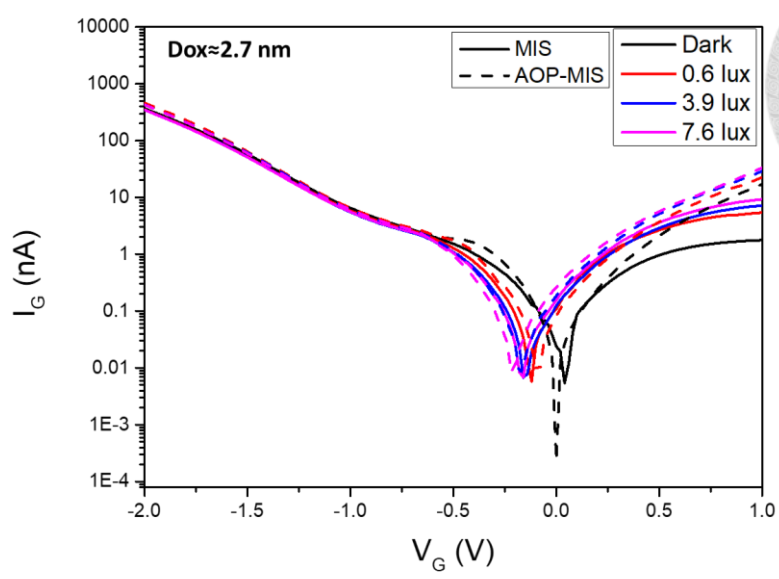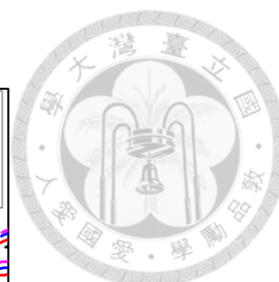li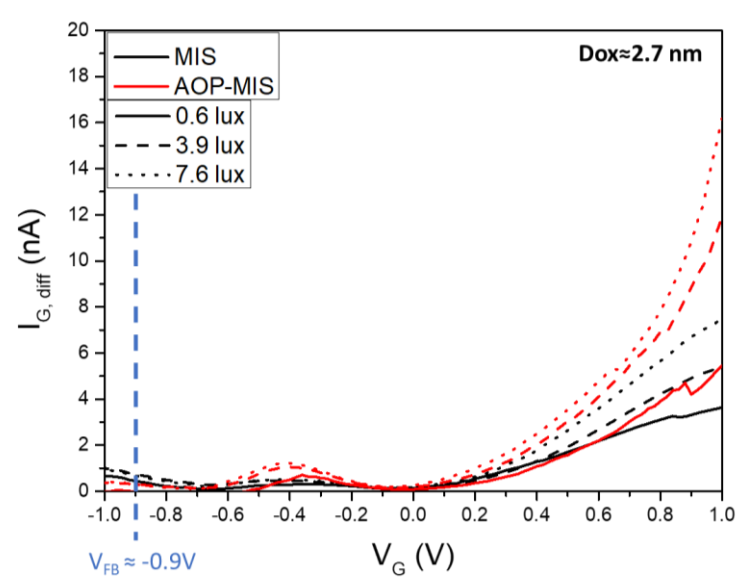ght illuminance (red: 0.6lux, blue: 3.9lux, pink: 7.6lux.) Noted that $C_{G,diff}$ is defined as $C_{G,diff} = C_{G,light} - C_{G,dark}$.

(a)

(b)

Figure 3-3. The comparison of (a) the dark and light currents and (b) $I_{G, diff}$-V_G of

MIS device (solid line) and AOP-MIS device (dash line) with 2.7nm oxide layer

under different light illuminance (red: 0.6lux, blue: 3.9lux, pink: 7.6lux.) Noted that

$I_{G, diff}$ is defined as $I_{G, diff} = I_{G, light} - I_{G, dark}$.

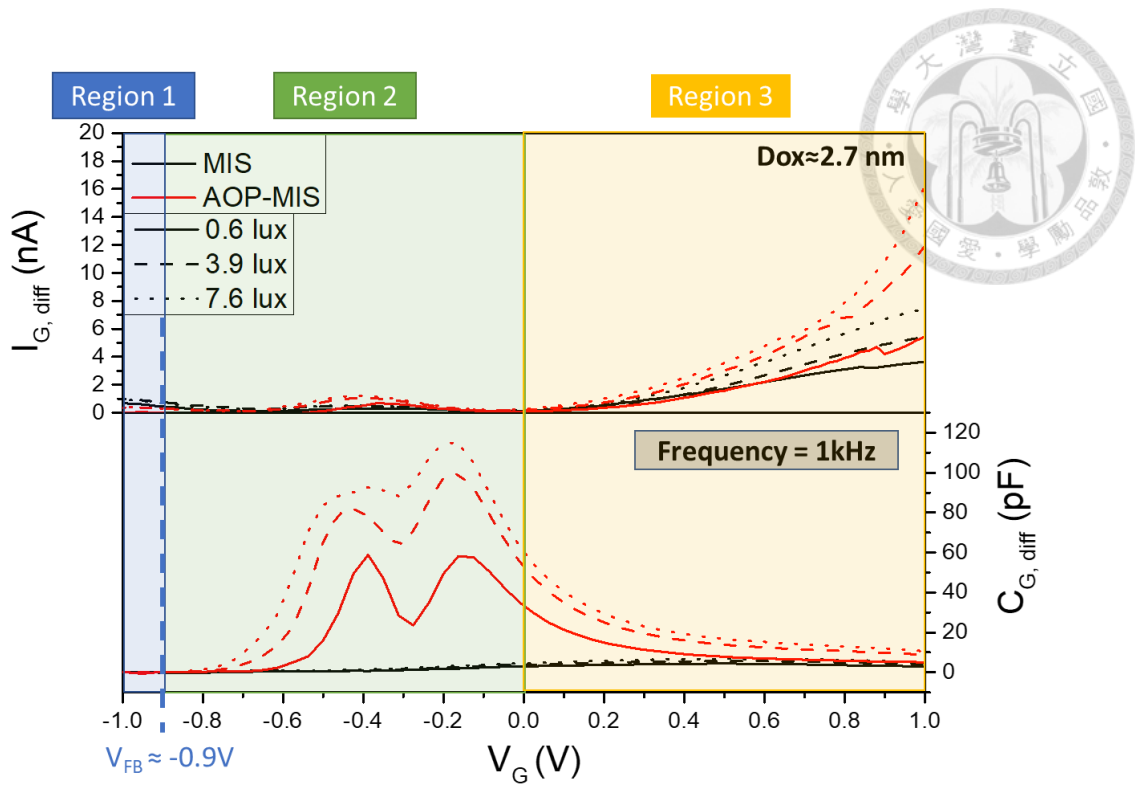**Figure 3-4.** The comparison of $I_{G,\,diff}$-V_G curves and $C_{G,\,diff}$-V_G curves of MIS device(black lines) and AOP-MIS device(red lines) with 2.7nm oxide layer under different illuminance of light. The discussion of behavior would be divided into three regions. Region 1 represented $V_G < V_{FB}$ (≈-0.9V), Region 2 represented $V_{FB} < V_G < 0$, and Region 3 represented $V_G > 0$.

Figure 3-5. The schematic diagrams of currents of (a) MIS device and (b) AOP-MIS

devices in region 1 ($V_G < V_{FB} = -0.9V$.)
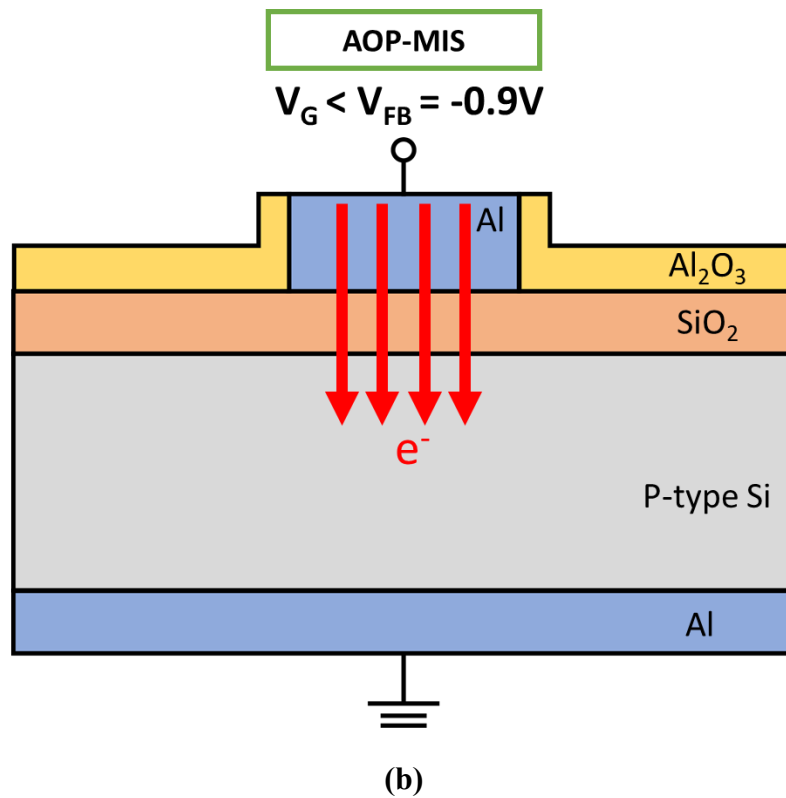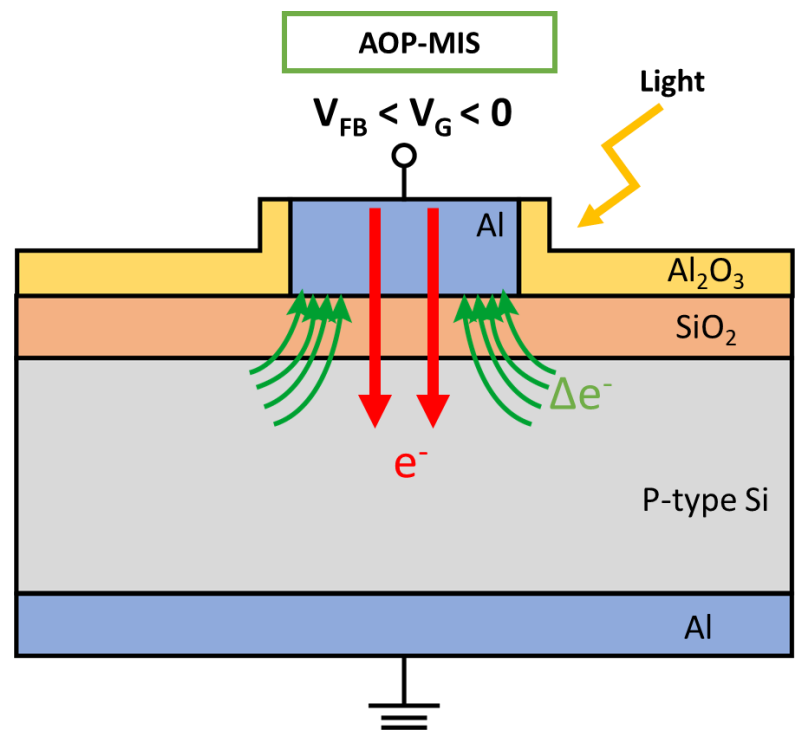
Figure 3-6. The schematic diagrams of currents of (a) MIS device and (b) AOP-MIS

devices with light in region 2 ($V_{FB} < V_G < 0$).

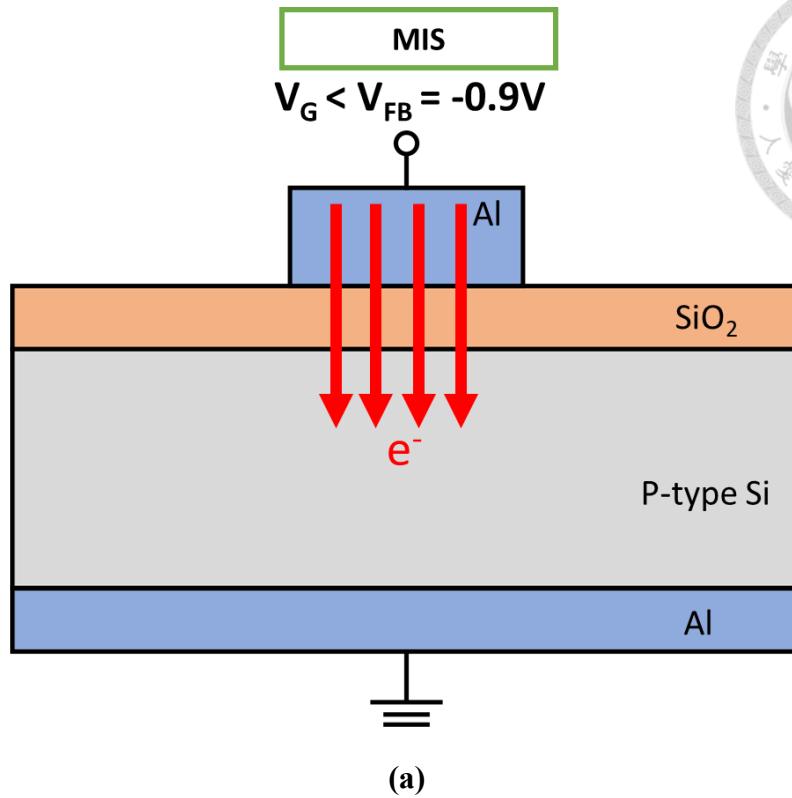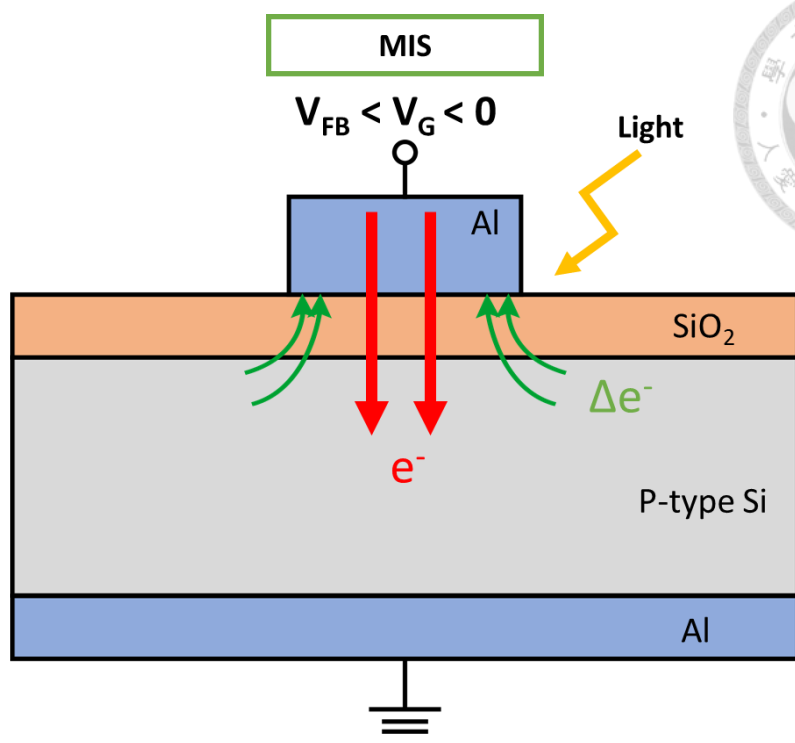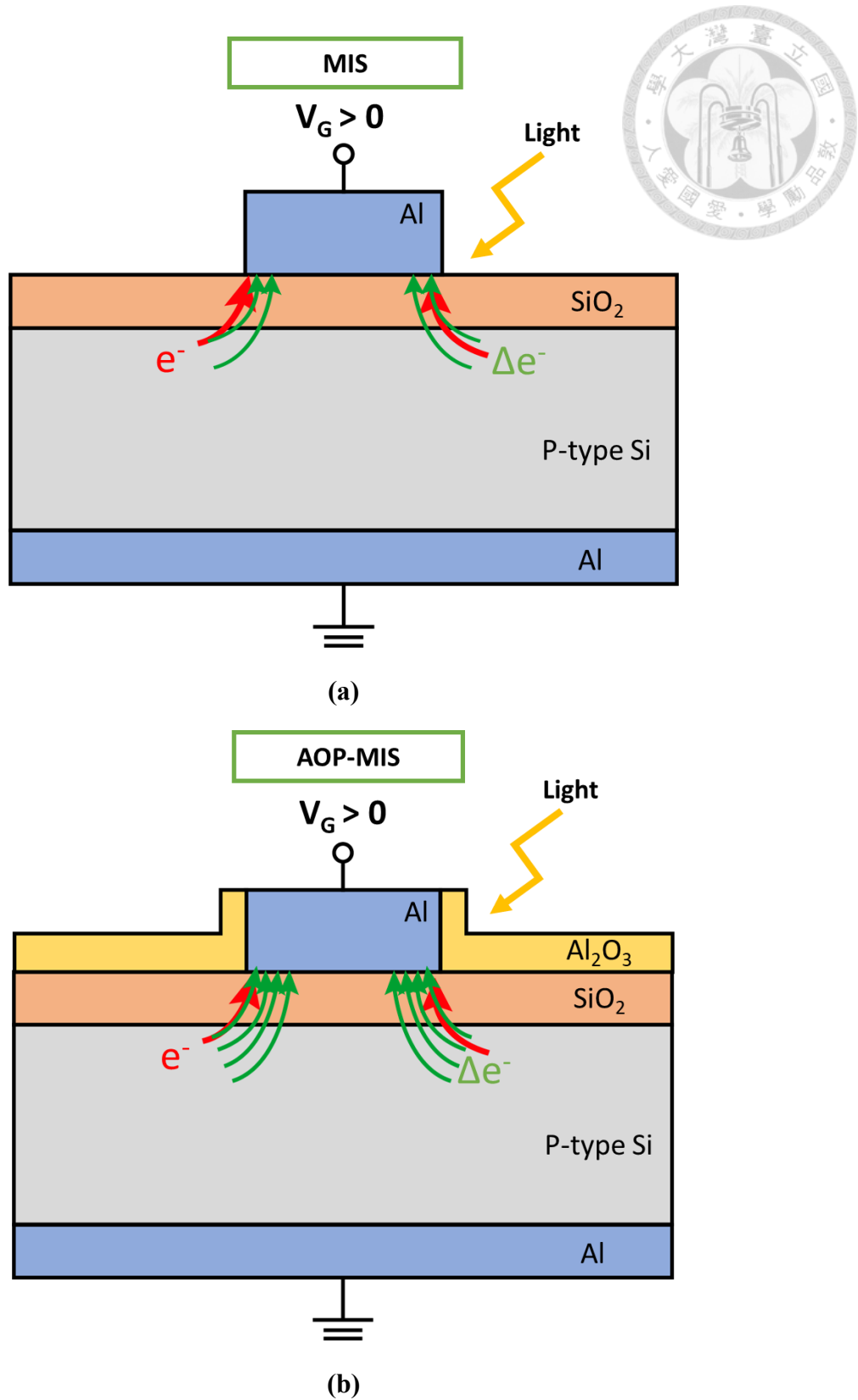**Figure 3-7. The schematic diagrams of currents of (a) MIS device and (b) AOP-MIS devices in region 3 ($V_G > 0$.)**
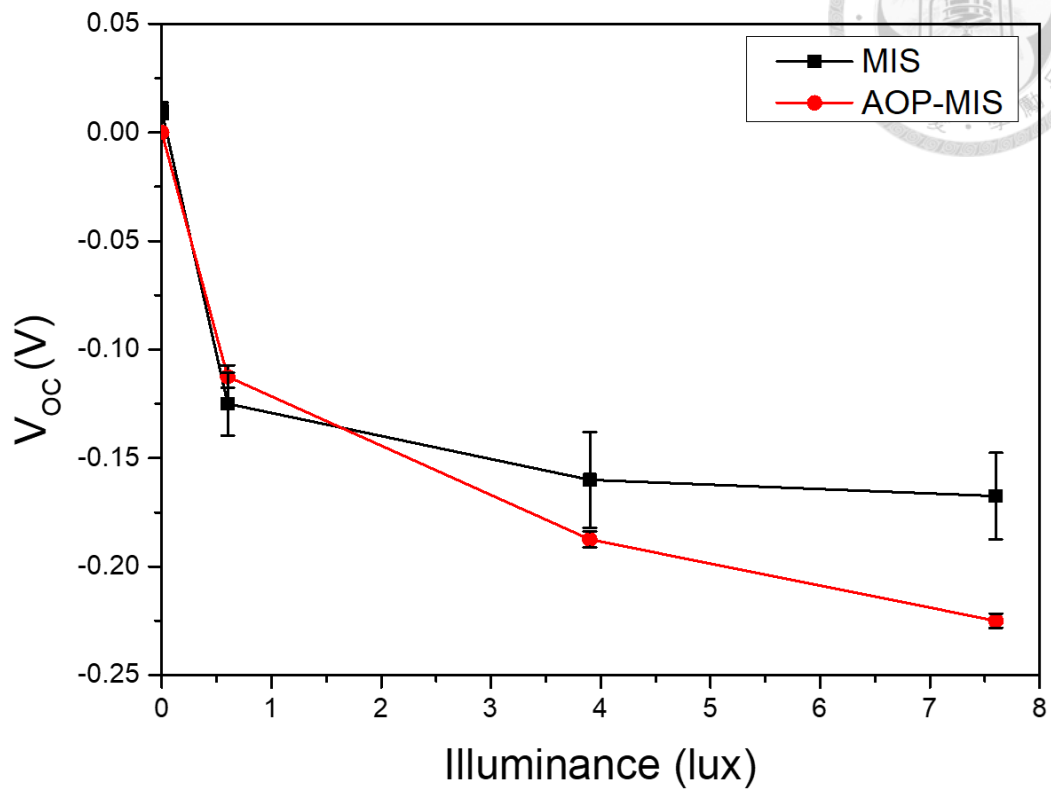
Figure 3-8. Comparison of V$_{oc}$-Illuminance of MIS and AOP-MIS devices where V$_{oc}$ is the open circuit voltage.

51
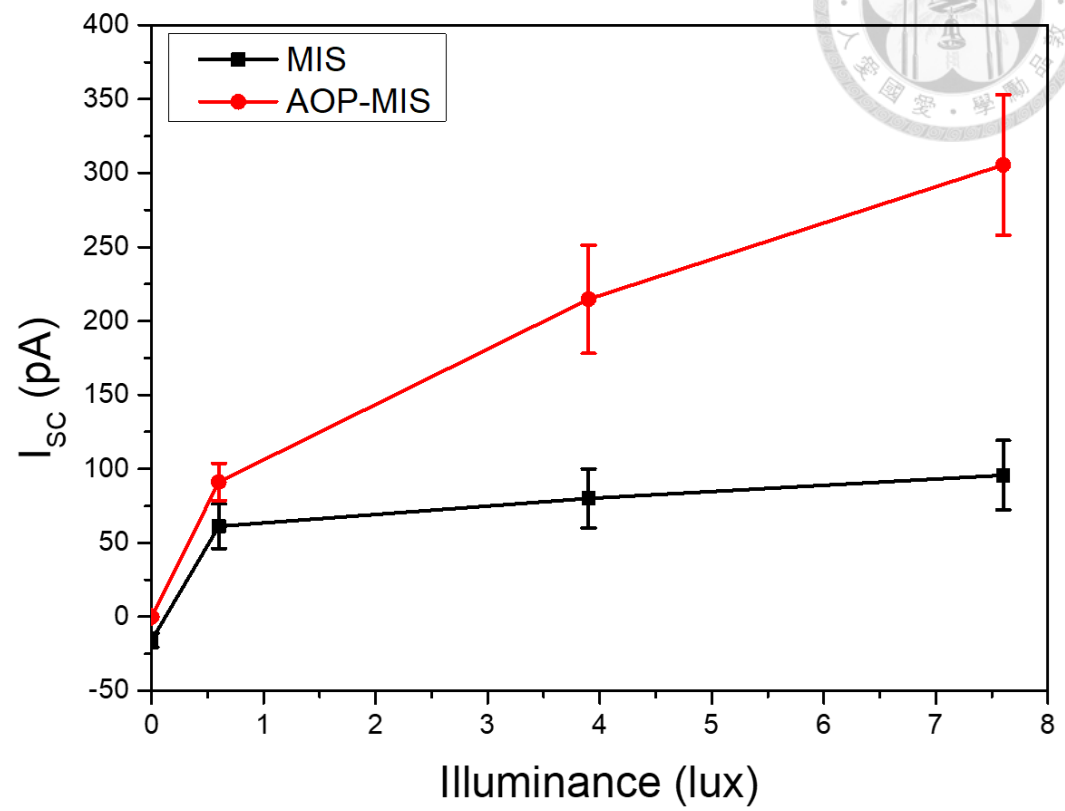
Figure 3-9. Comparison of I_{sc}-Illuminance of MIS and AOP-MIS devices where I_{sc} is the short circuit current.
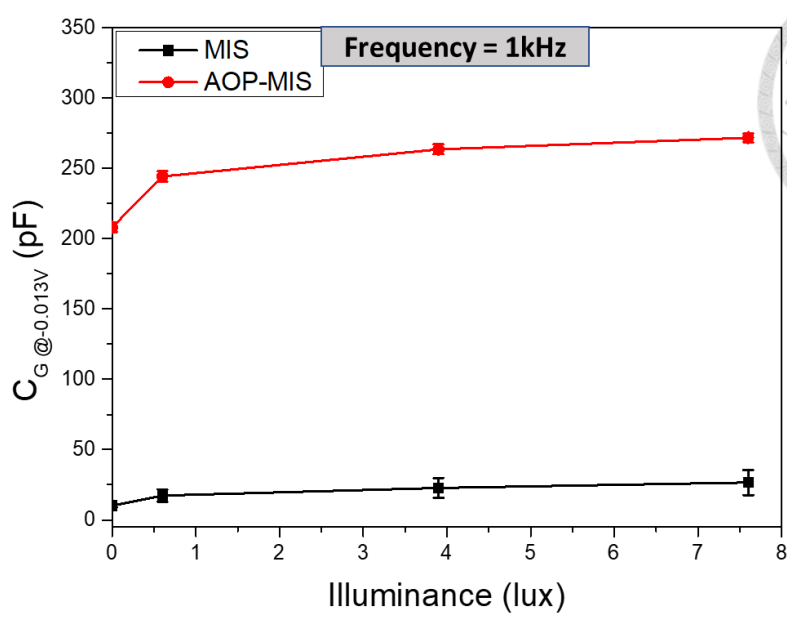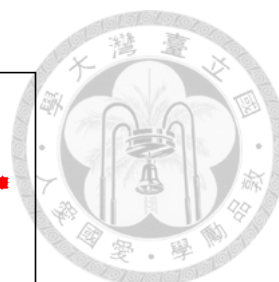
(a)
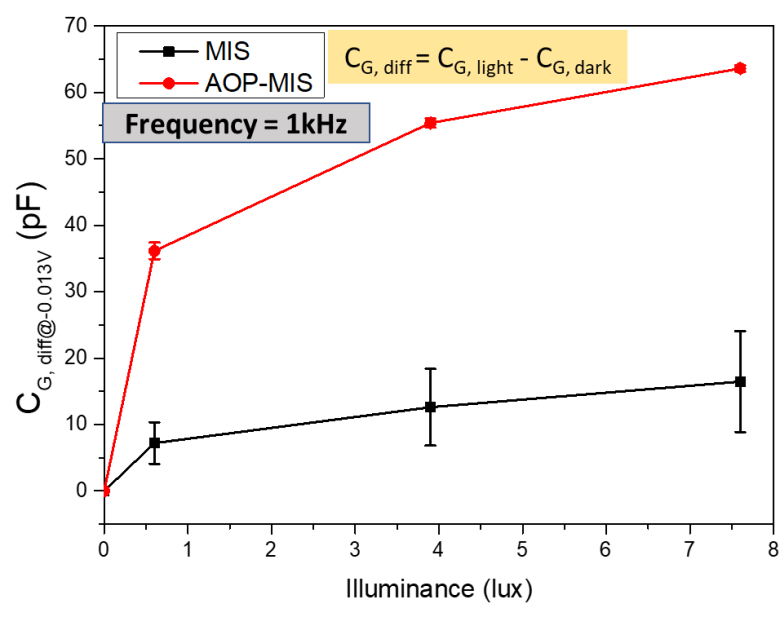
(b)

Figure 3-10. Comparison of the (a) capacitance C_G -V_G and (b) $C_{G, diff}$-V_G curves when V_G was near 0 V of MIS and AOP-MIS devices. Noted that $C_{G, diff}$ is defined as $C_{G, diff} = C_{G, light} - C_{G, dark}$.
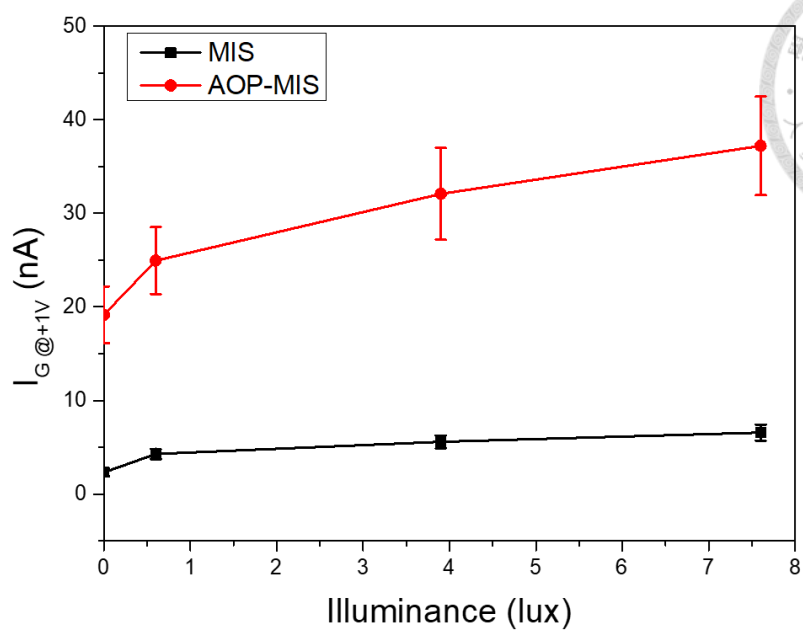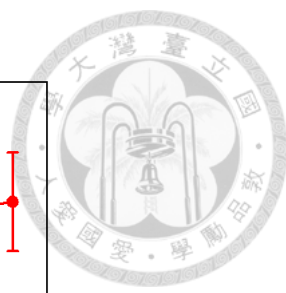
(a)
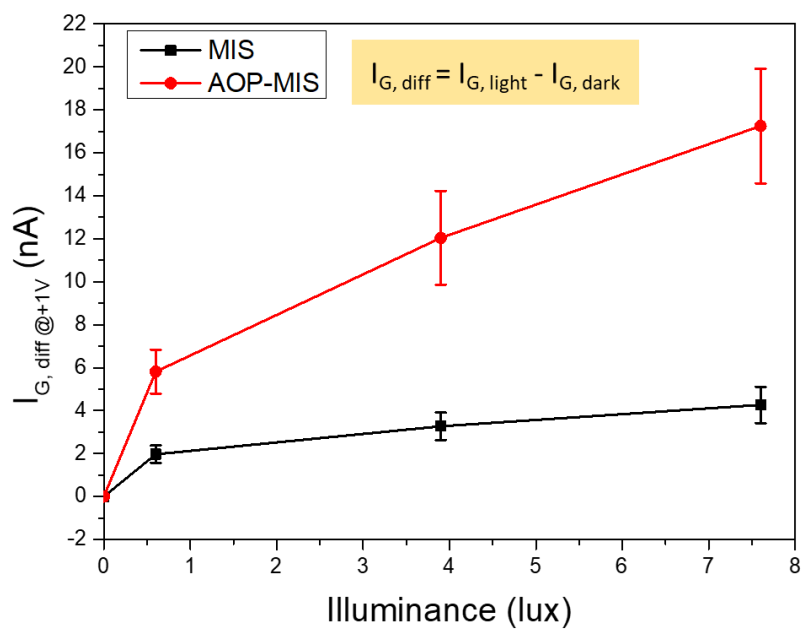
(b)

Figure 3-11. Comparison of the (a) gate current I_G -V_G and (b) $I_{G, diff}$-V_G curves when

V_G = +1V of MIS and AOP-MIS devices. Noted that $I_{G, diff}$ is defined as $I_{G, light}$ - $I_{G, dark}$.

54

Chapter 4
Conclusion and Future Work

4-1 Conclusion

4-2 Future Work
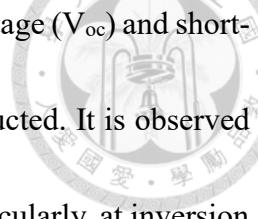
4-2-1 Thickness Dependence of Al_2O_3 Layer and Mechanism Analysis

4-2-2 IGOS Operating AOP-MIS Device

4-1 Conclusion

In this thesis, a novel structure of MISTD surrounding by an Al_2O_3-passivation layer was proposed. In Chapter 1, some fundamental knowledge of fabrication method and electrical characteristics of MISTD were provided. Then, in Chapter 2, the detailed fabrication process flow of AOP-MIS devices was presented. The measured C_G-V_G curves showed the result that with the help of the Al_2O_3 passivation layer, there were more minority carriers in inversion region and making the deep depletion effect suppressed comparing to conventional MISTD. Also, it was found that although the current behavior seemed to be similar for MIS devices and AOP-MIS devices in accumulation region, the inversion current was significantly larger for AOP-MIS device. The mechanism of this phenomenon was discussed. The Al_2O_3-passivation layer enhances local electric field, which leads to more voltage drop on oxide layer on the edge. With the enlarged V_{ox}, the Schottky barrier height that the holes face decreased accordingly. By the SBH modulation theory, the current was enhanced correspondingly. In Chapter 3, the photo-sensing ability of AOP-MIS was measured. It is found that comparing to the saturation of light happening in MIS devices, the AOP-MIS can have larger difference capacitance and difference current under light and dark condition. In depletion and inversion region, due to the enhancement of local electric field by Al_2O_3 layer, there are more excess carriers generating by light can be gathered. Hence, for AOP-MIS devices, the ability of light

56

sensing could be strengthened. The measurements of open-circuit voltage (V_{oc}) and short-circuit voltage (I_{sc}) under different light illuminance were also conducted. It is observed that AOP-MIS devices have better sensitivity than MIS devices. Particularly, at inversion region at V_G = 1V, $I_{G,diff}$ of AOP-MIS devices was four times higher than that of MIS devices.

4-2 Future Work

4-2-1 Thickness Dependence of Al_2O_3 Layer and Mechanism Analysis

Although the influence of Al_2O_3 passivation layer has been studied in this work, the relations between Al_2O_3 thickness and electrical characteristic is still not fully understood. However, the fabrication process used in this thesis faced an obstacle that the thickness of Al_2O_3-passivation layer cannot be well controlled due to the uneven etching rate of wet etching. Consequently, depositing Al layer of electrode region and surrounding region separately by process such as ALD, rather than etching, followed by oxidation process may provide a better solution to control the thickness. Moreover, in previous studies [27], it was found that by using anodization method, the surface of aluminum oxide layer becomes smoother, and oxygen vacancies within it could be recovered. Therefore, an aluminum oxide layer grown by anodization process may take into consideration to have a better quality of passivation layer. Also, aside from experimental results, simulation by TCAD is also an ideal method to verify the proposed model of mechanism behind this

novel structure, which may provide us more inspiration on how to further optimize the device structure.

4-2-2 IGOS Operating AOP-MIS Device

In Section 1-5, some researches of MIS devices with additional outer control ring were introduced. It was shown that IGOS device has a better performance of light sensing than single MISTD and ISOG device [21]. Therefore, combining AOP layer, which can enhance local electric field at the edge of device, to the IGOS device, the sensitivity of light may be able to further increased. The proposed structure is as shown in Fig. 4-1, containing an AOP layer surrounding the outer ring to strengthen the electric field which could lead to the enhancement of light sensitivity.
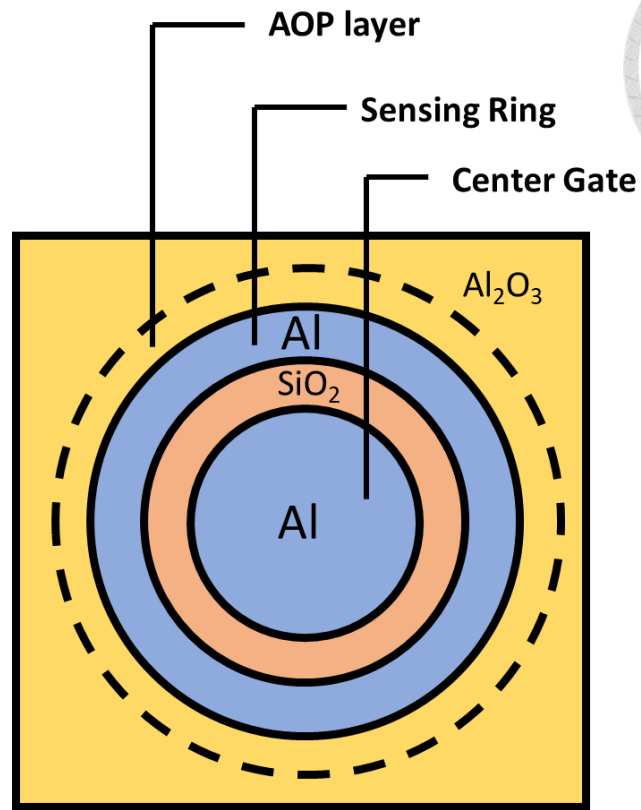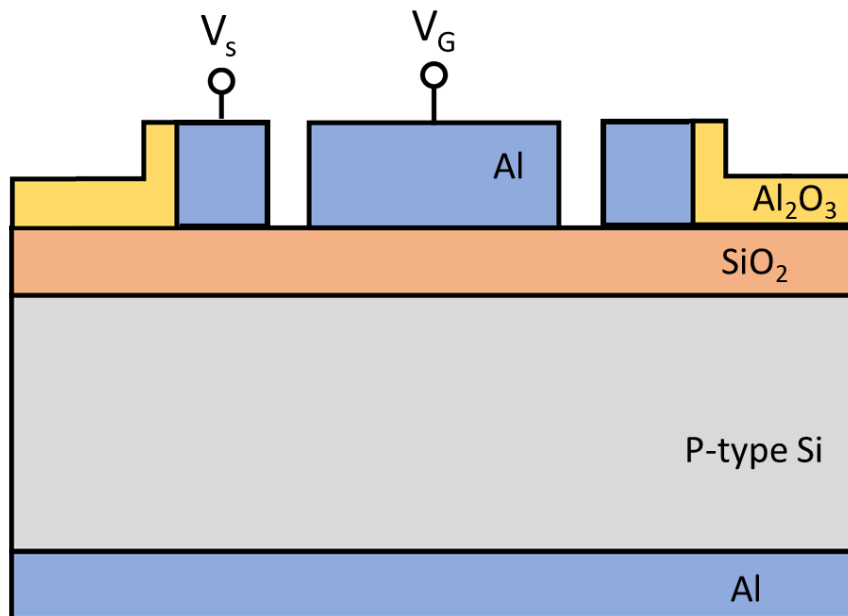
Figure 4-1. Schematic diagram of (a)top view and (b)cross section of proposed IGOS operating AOP-MIS device.

Reference

[1] G. E. Moore, "Cramming more components onto integrated circuits," *IEEE Solid-State Circuits Soc. Newslett.*, vol. 11, no. 3, pp. 33-35, Jan. 2006.

[2] C. S. Liao and J. G. Hwu, "Subthreshold Swing Reduction by Double Exponential Control Mechanism in an MOS Gated-MIS Tunnel Transistor," *IEEE Transactions on Electron Devices*, vol. 62, no. 6, pp. 2061-2065, June 2015.

[3] S. Yen-Hao and H. Jenn-Gwo, "An on-chip temperature sensor by utilizing a MOS tunneling diode," *IEEE Electron Device Letters*, vol. 22, no. 6, pp. 299-301, 2001.
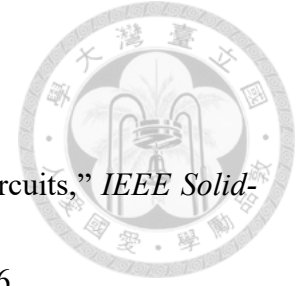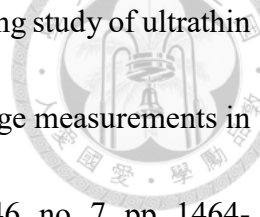
[4] T. M. Wang, C. H. Chang and J. G. Hwu, "Enhancement of Temperature Sensitivity of Metal-Oxide-Semiconductor (MOS) Tunneling Temperature Sensors by Utilizing Hafnium Oxide (HfO2) Film Added on Silicon Dioxide (SiO2)," *IEEE Sens. J.*, vol. 6, no. 6, pp. 1468-1472, Dec. 2006.

[5] D. Beckmeier and H. Baumgärtner, "Metal-Oxide-Semiconductor Diodes Containing C60 Fullerenes for Non-volatile Memory Applications," *J. Appl. Phys.*, vol. 113, no. 4, pp. 044520, Jan. 2013.

[6] T. Y. Chen and J. G. Hwu, "Two States Phenomenon in the Current Behavior of Metal-Oxide-Semiconductor Capacitor Structure with Ultra-Thin SiO$_2$," *Appl. Phys. Lett.*, vol. 101, no. 7, pp. 073506, Aug. 2012.

[7] W. C. Chen, C. F. Yang and J. G. Hwu, "Enhanced Two States Current in MOS-

Gated MIS Separate Write/Read Storage Device by Oxide Soft Breakdown in Remote Gate," *IEEE Trans Nanotechnol*, vol. 18, pp. 62-67, Nov. 2018.

[8] C. W. Liu, W. T. Liu, M. H. Lee, W. S. Kuo, and B. C. Hsu, "A novel photodetector using MOS tunneling structures," *IEEE Electron Device Letters*, vol. 21, no. 6, pp. 307-309, 2000.

[9] P. F. Schmidt and W. Michel, "Anodic Formation of Oxide Films on Silicon," *J. Electrochem. Soc.*, vol. 104, pp. 230-236, 1957.

[10] C. C. Ting, Y. H. Shih, and J. G. Hwu, "Ultralow Leakage Characteristics of Ultrathin Gate Oxides (~3nm) Prepared by Anodization Followed by High-Temperature Annealing," *IEEE transactions on Electron Devices*, vol. 49, no. 1, January 2002.

[11] E. H. Nicollian and J. R. Brews, "MOS (Metal Oxide Semiconductor) Physics and Technology," John Wiley & Sons, New York, 1981, ch. 3.

[12] R. Tsu, L. Esaki, "Tunneling in a Finite Superlattice", *Appl. Phys. Lett.*, vol. 22, no.11, pp.562, March 1973.

[13] C. H. Chen, K. C. Chuang, J. G. Hwu, "Characterization of Inversion Tunneling Current Saturation Behavior for MOS (p) Capacitors with Ultrathin Oxides and High-k Dielectrics," *IEEE Trans. Electron Devices*, vol. 56, no. 6, pp.1262-1268, June 2009.

[14] N. Yang, W. K. Henson, J. R. Hauser and J. J. Wortman, "Modeling study of ultrathin gate oxides using direct tunneling current and capacitance-voltage measurements in MOS devices," *IEEE Transactions on Electron Devices*, vol. 46, no. 7, pp. 1464-1471, Jul. 1999.

[15] Wen-Chin Lee and Chenming Hu, "Modeling CMOS tunneling currents through ultrathin gate oxide due to conduction- and valence-band electron and hole tunneling," *IEEE Transactions on Electron Devices*, vol. 48, no. 7, pp. 1366-1373, Jul. 2001.

[16] Y. P. Lin and J. G. Hwu, "Oxide-Thickness-Dependent Suboxide Width and Its Effect on Inversion Tunneling Current," *J. Electrochem. Soc.*, vol. 151, no. 12, pp. G853–G857, Oct. 2004.

[17] Y. K. Lin and J. G. Hwu, "Role of lateral diffusion current in perimeter-dependent current of MOS(p) tunneling temperature sensors," *IEEE Trans. Electron Devices*, vol. 61, no. 10, pp. 3562–3565, Oct. 2014.

[18] S. M. Sze and K. K. Ng, *Physics of Semiconductor Devices*. Hoboken, NJ, USA: Wiley, 2007.

[19] Y. K. Lin and J. G. Hwu, "Photosensing by Edge Schottky Barrier Height Modulation Induced by Lateral Diffusion Current in MOS(p) Photodiode," *IEEE Transactions on Electron Devices*, vol. 61, no. 9, pp. 3217-3222, Sept. 2014.

[20] W. T. Hou and J. G. Hwu, "Photo response enhancement in MIS(p) tunnel diode via coupling effect by controlling neighboring device inversion level," *ECS J. Solid State Sci. Technol.*, vol. 6, no. 10, pp. Q143–Q147, Nov. 2017, doi: 10.1149/2.0031712jss.

[21] C. Y. Huang and J. G. Hwu, "Enhanced Photo Sensing and Lowered Power Consumption in Concentric MIS Devices by Monitoring Outer Ring Open-Circuit Voltage With Biased Inner Gate," *IEEE Transactions on Electron Devices*, vol. 68, no. 7, pp. 3417-3423, July 2021.

[22] P. J. Price and J. M. Radcliffe, "Esaki Tunneling," *IBM Journal of Research and Development*, vol. 3, no. 4, pp. 364-371, Oct. 1959.

[23] W. Shockley and W. T. Read, "Statistics of the Recombinations of Holes and Electrons," *Phys. Rev.*, vol. 87, no. 5, pp. 835–842, Sep. 1952.

[24] R. N. Hall, "Electron-Hole Recombination in Germanium," *Phys. Rev.*, vol. 87, no. 2, p. 387, July 1952.

[25] J. Dziewior and W. Schmid, "Auger coefficients for highly doped and highly excited silicon," *Appl. Phys. Lett.*, vol. 31, no. 5, pp. 346–348, Sep. 1977.

[26] G. Iannaccone, G. Curatola, and G. Fiori, "Effective Bohm Quantum Potential for device simulators based on drift-diffusion and energy transport," in *Simulation of Semiconductor Processes and Devices*. Vienna, NY, USA: Springer, 2004, pp. 275–

278.

[27] J. C. Lin (2022). "Study of Nonvolatile Memory in Coupled MIS(p) TD with

Anodization-Compensated Al_2O_3 Dielectric," Unpublished Master Thesis, National

Taiwan University, Taipei, Taiwan.